Statistical analysis of the ionospheric response during storm conditions over South Africa using ionosonde and GPS data

A thesis submitted in fulfillment of the
requirements for the degree of

MASTER OF SCIENCE

of

RHODES UNIVERSITY

by

Tshimangadzo Merline Matamba

December 2014

Abstract

Ionospheric storms are an extreme form of space weather phenomena which affect space- and ground-based technological systems. Extreme solar activity may give rise to Coronal Mass Ejections (CME) and solar flares that may result in ionospheric storms. This thesis reports on a statistical analysis of the ionospheric response over the ionosonde stations Grahamstown (33.3°S, 26.5°E) and Madimbo (22.4°S,30.9°E), South Africa, during geomagnetic storm conditions which occurred during the period 1996 - 2011. Total Electron Content (TEC) derived from Global Positioning System (GPS) data by a dual Frequency receiver and an ionosonde at Grahamstown, was analysed for the storms that occurred during the period 2006 - 2011. A comprehensive analysis of the critical frequency of the F2 layer (foF2) and TEC was done. To identify the geomagnetically disturbed conditions the Disturbance storm time (Dst) index with a storm criteria of Dst ≤ -50 nT was used. The ionospheric disturbances were categorized into three responses, namely single disturbance, double disturbance and not significant (NS) ionospheric storms. Single disturbance ionospheric storms refer to positive (P) and negative (N) ionospheric storms observed separately, while double disturbance storms refer to negative and positive ionospheric storms observed during the same storm period. The statistics show the impact of geomagnetic storms on the ionosphere and indicate that negative ionospheric effects follow the solar cycle. In general, only a few ionospheric storms (0.11%) were observed during solar minimum. Positive ionospheric storms occurred most frequently (47.54%) during the declining phase of solar cycle 23. Seasonally, negative ionospheric storms occurred mostly during the summer (63.24%), while positive ionospheric storms occurred frequently during the winter (53.62%). An important finding is that only negative ionospheric storms were observed during great geomagnetic storm activity (Dst ≤ -350 nT). For periods when both ionosonde and GPS was available, the two data sets indicated similar ionospheric responses. Hence, GPS data can be used to effectively identify the ionospheric response in the absence of ionosonde data.

Acknowledgement

Firstly, I would like to express my sincere gratitude to my supervisors, Dr John Bosco Habarulema and Dr Lee-Anne McKinnell, for their continual guidance and support throughout the duration of this study. Dr Lee-Anne McKinnell provided me with assistance and encouragement during my MSc study. I greatly appreciate Dr John Bosco Habarulema, my supervisor for his patience, motivation and knowledge.

I thank Dr Pierre Cilliers and Mrs Jeanne Cilliers for their love, support and help to make my stay in Hermanus a fruitful experience. They were like family to me. To Dr Pierre Cilliers, thank you for assisting me with MATLAB. I much appreciate the contribution by the researchers, staff and students at SANSA Space Science. I also thank Mrs Anita Engelbrecht for her maternal love and comfort throughout my stay at SANSA. I also acknowledge Mrs Delray Janse van Rensburg and Mrs Jeanne Cilliers for their work in editing this thesis.

To Mrs Electdom Matandirotya and Mpho Tshisaphungo, thank you for both your friendship and encouragement. I thank my office mates (Vumile, Nigusie, Thina, Amin, Jean, Tsige), and Ahoua, Fenni, Emirant for their contributions.

I am very grateful to SANSA Space Science, Hermanus for hosting me during my studies and for providing financial assistance for my research. My acknowledgements would not be complete without mentioning the support of role played by Professor Saalih Allie and Dr Victoria Ikoro. I also wish to acknowledge Dr Dalia Buresova for her contribution.

I will always remember the enormous encouragement by my husband, daughter, Mrs Magadze M.M, Mr Matamba M.A, my siblings and my mother in Law, Vho-Merina. I wish to thank my family for their love and moral support.
Most of all, I wish to thank my Heavenly Father for His guidance and protection.

Dedication

This thesis is dedicated to my husband, Thingahangwi, daughter, Vhugala, Mrs Magadze, my late parents Johannah and Solomon, and my late uncle, Mr Magadze.

Contents

List of Figures

List of Tables

Acronyms

AE	Auroral Electrojet
CIR	Corotating Interaction Region
CME	Coronal Mass Ejection
Dst	Disturbance storm time
EIA	Equatorial Ionisation Anomaly
EUV	Extreme Ultraviolet radiation
foF2	Critical Frequency of F2 layer
GNSS	Global Navigational Satellite System
GPS	Global Positioning System
HF	High Frequency
hmF2	Maximum peak height
HSSs	High speed streams
ICME	Interplanetary Coronal Mass Ejection
IMF	Interplanetary Magnetic Field
IPP	Ionospheric Pierce Point
Ne	electron density
N_{max}	Maximum electron density
NGA	National Geospatial-intelligence Agency
nT	nanoteslas
PPEF	Prompt Proton Electric Field
SI	Sudden Impulse
SAO	Standard Archiving Output
SSC	Sudden Storm Commencement
STEC	Slant Total Electron Content
TAD	Traveling Atmospheric Disturbance
TEC	Total Electron Content
TECU	TEC unit
TID	Traveling Ionospheric Disturbance
TRACE	Transition Region and Coronal Explorer
USDoD	United States Department of Defence
VTEC	Vertical Total Electron Content

Chapter 1

Introduction

The ionosphere is the region of ionised plasma extending from about 50 to 1200 km above the Earth's surface. It consists of free electrons and ions produced during interaction of EUV radiation with upper atmosphere neutral gas. It comprises of four layers during the day at different altitudes, namely D, E, F1 and F2. At night the D and F1 layers disappear, leaving only the E and F2 layers. The ionosphere is not stable, it varies with time of day, height, geographic or geomagnetic location, season as well as solar activity. Solar activity such as CME and solar flares may result in ionospheric storms. Ionospheric storms are caused by a cloud of plasma ejected from a large solar flare that hits the Earth (McNamara, 1991). During an ionospheric storm there is a change in the electron density of the ionosphere, hence it affects ionospheric parameters.

Structures in the ionosphere may negatively affect technology such as communication systems. Ionospheric storms are an extreme form of space weather which may affect space-borne and ground-based technological systems. Space weather refers to conditions on the Sun, in the solar wind, magnetosphere, ionosphere and thermosphere. Adverse conditions in the space environment may cause disruption of satellite operations, communications, navigation, and electric power distribution grids, which may lead to socio-economic losses (Moldwin, 2008).

Geomagnetic storms are the result of transient solar phenomena on the Sun and are often the source of interplanetary magnetospheric disturbances. The increase and decrease in electron density are termed positive and negative ionospheric storms respectively. Positive and negative ionospheric storms are believed to be caused, among other factors, by TAD and by a change in neutral composition respectively (Richmond and Roble, 1979; Prölss, 1995, 2004; Schunk and Nagy, 2009). In mid-latitude regions, both an increase and a decrease in the electron density may occur during a geomagnetic storm.

The focus of this research is to describe and discuss the ionospheric response during geomagnetic storms over South Africa. This was done by studying the responses of the foF2

over Grahamstown ($33.3^oS, 26.5^oE$) and Madimbo ($22.4^oS, 30.9^oE$) ionosonde stations, and the TEC derived from the GPS dual frequency receiver measurements over Grahamstown during geomagnetic storms.

1.1 Problem statement

Significant research on the ionospheric response during disturbed conditions has been conducted on individual geomagnetic storms over South Africa, using ionospheric parameters such as TEC, foF2, Nmax and hmF2 (Amabayo et al., 2012; Katamzi et al., 2012; Ngwira et al., 2012b; Habarulema et al., 2013b; Yao et al., 2013; Katamzi and Habarulema, 2014). However, no comprehensive statistical analysis has done for South Africa and therefore, it is the focus of this study. Statistical studies similar to this one exist for other mid-latitude regions.

A statistical study of the storm effects in the middle and low latitude ionosphere in the East Asian sector during 515 geomagnetic storms was done using the foF2 data observed at 4 ionosonde stations for the period of 1957 - 2006 (Gao et al., 2008). Statistics of geomagnetic storms and ionospheric storms at Kokubunji (35.7^oN, 139.5^oE; 26.8^oN magnetic latitude) in Japan and Boulder (40.0^oN, 254.7^oE; 47.4^oN) in America during two solar cycles (22 and 23), that is from 1985 - 2005, using maximum electron density (Nmax), were reported. Different types of ionospheric storms were observed and also their variation with local time, season and solar cycle (Vijaya Lekshmi et al., 2011).

1.2 Primary research objectives

This work addresses the construction of a data base that would be useful in modeling ionospheric behaviour during storm conditions. The aim of this thesis is to:

- Identify geomagnetic storms which occurred during the period 1996 to 2011, using the criterion of the Dst ≤ -50 nT.
- Investigate the ionospheric response (foF2 and TEC) to geomagnetic activity during the above period, using South African data.

1.3 Thesis overview

This thesis comprises five Chapters. Chapter 1 is an introduction, Chapter 2 details the theoretical background to ionospheric storms, their sources and their interaction with the

Earths upper atmosphere, Chapter 3 describes the ionospheric data sources used, Chapter 4 presents the statistics of the ionospheric storms and their discussion and Chapter 5 offers the conclusion and suggestions for future work.

Chapter 2

The Sun, ionosphere and ionospheric storms

2.1 Introduction

This chapter gives a detailed background to causes of ionospheric storms. The Sun and the solar activity that may lead to ionospheric storms and geomagnetic disturbances are also discussed.

2.2 The Sun

The Sun is our closest star and source of energy and controls both space climate and space weather. It was formed 4.55×10^9 years ago and has a mass of 2.0×10^{30} kg, radius 7.0×10^{10} cm, volume of 1.412×10^{27} m^3, effective black body temperature of 5778 K, density of 1.4 g/ cm^3, and luminosity (energy radiated per unit time) of 3.84×10^{26} W (Kutner, 2003; Koskinen, 2011). The Sun comprises different surfaces, namely the corona, chromosphere, photosphere, convection zone, radiation zone, and the core where nuclear fusion takes place. The chemical composition is approximately 94% hydrogen, 6% helium and 0.1% other elements. All these constituents are in an ionized state as the Sun is a gaseous body (Prölss, 2004; Kutner, 2003).

The solar atmosphere contains magnetic fields which are generated in the solar interior. The tachocline, a transiting region of the Sun between the radiative interior and the differentially rotating outer convective zone, plays an important role in the behavior of the observed dynamics (Miesch, 2005).

2.2.1 Solar wind

The solar wind is the stream of particles (positive ions and electrons) that are emitted from the Sun into interplanetary space. This stream is a result of the pressure difference between

the solar corona and interplanetary space which drives the solar plasma radially outward, escaping from the influence of solar gravity. The particles have a density of $5 - 10$ cm^3. At 1.49×10^8 km from the Sun to the observer, the solar wind makes an angle of roughly 45 degrees. The complex structure of the solar magnetic field reduces to a radially directed structure less than 14×10^{10} km away from the photosphere. The solar wind magnetic field is frozen into the solar wind plasma due to high conductivity of the solar wind. It is transported outward into the interplanetary medium (Kamide and Chian, 2007).

The solar wind is affected strongly by changes in solar activity, and it transmits the effects of solar variability to the planets, including the Earth. There are two types of solar wind, the fast and slow solar wind. The fast solar wind originates from the coronal holes where the magnetic field is open, and has a velocity of between 400 and 800 km/s. On the other hand, the slow solar wind originates from the regions close to the heliospheric current sheet at the heliomagnetic equator during solar minimum. During solar maximum the slow solar wind originates above the coronal helmet streamers in active regions where the magnetic field lines are closed. The slow and fast solar winds collide at a certain distance from the Sun and an interactive region develops between the slow and fast streams. These structures rotate with the Sun and are called CIRs (Kamide and Chian, 2007).

The solar wind may have an effect on Earth, but most of the solar wind particles directed at Earth never reach the surface of the Earth. This is because the Earth is shielded from the charged particles by an invisible force field known as Earth's magnetic field. The charged particles cannot travel across the field lines, and so the particles travel along the field lines. The increased abundance of charged particles in the atmosphere creates radio interference (Kutner, 2003).

The solar energy is transferred to the ionosphere in two ways. Solar radiation in the ultraviolet range is directly absorbed by the sunlit ionosphere and is responsible for the undisturbed ionosphere. The solar wind energy is captured by the magnetosphere and is transformed and dissipated in the polar ionosphere. This energy source is responsible for the disturbed ionosphere (Prölss, 1995).

The intensity of solar wind energy is described in terms of geomagnetic activity indices. These indices correspond with the observed dissipation effects and they are easily accessible as will be discussed in Chapter 3.

2.3 Sunspot and solar activity cycle

Sunspots are the dark regions on the Sun's surface. They are dark because they are cooler (≈3000 K) than the area around them (5778 K). Sunspot life varies, some last for a few days, while others last for four to five solar rotations. They regularly occur in groups, one group can contain a single or dozens of spots. The spots rotate with the Sun from east to west, and the Sun rotates in the same direction as the Earth even though the Earth is a rigid body. The sunspots have periodic variations of high and low activity that repeat approximately every 11 years. The occurrence of sunspots is measured by the Wolf or Zuric sunspot number R, given by:

$$R = k(10g + s) \tag{2.1}$$

where g is the number of sunspot groups, s is the number of individual spots observed and k is the correction factor which takes into account the observer's characteristics and the equipment. Sunspots occur at different solar latitudes. After sunspot minimum, at sunspot maximum and during the declining phase the spots occur at latitudes of 20° to 30° north and south, ±15° and in latitudes of 5° to 10° respectively (Davies, 1990).

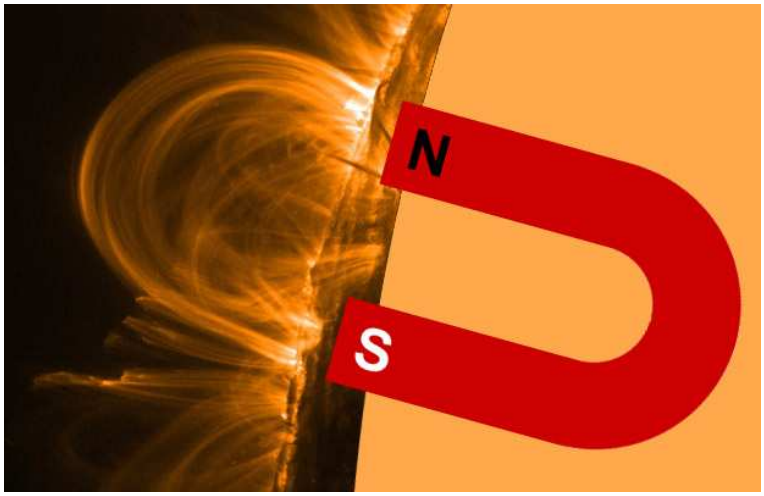

Figure 2.1: A giant horseshoe magnet inside of the Sun, demonstrating how sunspots tend to occur in pairs. One sunspot is like the North pole of a magnet; the other sunspot is like a South pole. Credit: Windows to the Universe, original artwork by Randy Russell (19 January 2010) using an image from NASA's TRACE (Transition Region and Coronal Explorer) spacecraft.

Sunspots are caused by strong magnetic fields on the Sun. They tend to occur in pairs and have bipolar magnetic fields, meaning they have both negative and positive magnetic polarity. The leading spots in sunspot groups have one polarity for almost all northern hemisphere groups and the opposite in the southern hemisphere groups, as illustrated in Figure 2.1.

The sunspot polarities reverse from one 11-year cycle to the next leading to a 22-year solar cycle. The magnetic configurations on the Sun vary in periods ranging from days to years. Magnetic structures determine the region where and when the prominences, flares, CMEs, and filaments will occur (Davies, 1990).

2.3.1 Solar flare

Solar flares are large explosions on the Sun which take place in the solar corona and chromosphere. They mostly occur around the sunspots or active regions, when the magnetic energy that has built up in the solar atmosphere is suddenly released, thus during high solar activity. Flares vary in size and duration. Only those flares that arise from the part of the Sun aligned to the geometry of the Earth come torwards the Earth. They may cause disturbances in the ionosphere and to HF communication. Solar flares are responsible for X-rays, solar protons and a plasma cloud in the ionosphere (McNamara, 1991).

2.3.2 Coronal mass ejections

CMEs are another form of mass release from the Sun. They were first thought to be initiated by solar flares, but it is now known that they are not associated with flares (Cane, 1997). CMEs occur over a wider range of solar latitudes, while solar flares seemed to be restricted to lower latitudes. When the CME lifts off from a closed field line of the solar corona, the topology causes the superthermal electrons to move outward from both footprints, causing a counter-stream flux as a signature. Near solar maximum, about three to four CMEs are produced daily and one CME every five days near solar minimum. The faster CMEs have outward speeds of greater than 3000 km/s. The greatest CME that occurred during solar cycle 23 had a speed of about 3387 km/s and occurred on the 10^{th} of November 2004 (Gopalswamy, 2006; Uwamahoro, 2011). The faster CMEs produce large shock waves which accelerate electrons in the solar wind and produce radio waves (Gonzalez-Esparza and Aguilar-Rodriguez, 2009; ESA, 2015). Again the large shock waves accelerate atomic nuclei in the solar wind which produces the radiation storm.

The CMEs that impact the Earth's magnetosphere may cause severe geomagnetic storms which may lead to ionospheric disturbance. Geomagnetic storms occur when ICME and CIRs containing the southward magnetic field, arrive at the Earth's magnetosphere, resulting in a magnetic reconnection with the geomagnetic field (Gopalswamy, 2006).

2.4 The magnetosphere

The magnetosphere is the region of the Earth's atmosphere that is formed by the interaction of the solar wind and the Earth's magnetic field. The dynamics of the energetic particles and plasma within the magnetospheric cavity are strongly influenced by the geomagnetic field. Solar activity has a strong influence on the size and shape of the magnetosphere on both the day-side and night-side, and therefore, is the main driver of geomagnetic storms. The coupling between the ionosphere and the magnetosphere is important, because it allows the transfer of a large amount of energy into the ionosphere and at the same time the ionosphere provides an inner boundary (Walker, 2005; Ngwira, 2011).

Energy exchange between the plasma and the neutral particles maximizes in the E region, resulting in substantial Joule or frictional heating, which represents an important heat source for the neutral thermosphere. The variable auroral input alters the lower thermospheric composition and neutral winds. Sometimes impulsive heating lifts the constant pressure surfaces, launching TADs which propagate towards the equator (Buonsanto, 1999).

2.5 An overview of the ionosphere

The ionosphere is the ionised component of the upper atmosphere. It is formed when EUV radiation from the Sun strips electrons from the neutral atoms of the Earth's atmosphere. There are two processes which occur in the ionosphere, namely photoionisation and recombination. Photoionisation is the process in which a photon strips an electron from a neutral atom, creating a positively charged ion. Recombination, on the other hand, is a reverse of photoionisation, where negatively charged electrons and positively charged ions combine to form neutral atoms. Recombination is the main process in which electrons are lost in higher parts of the ionosphere, and in the lower parts electrons are lost by the process of attachment. The electrons attach to the neutral atoms and become negatively charged. The negative ions are heavier than electrons, and do not respond to the electromagnetic oscillations of the radio waves like the positively charged ions. Recombination and attachment occurs always at all levels of the ionosphere, whereas photoionisation only occurs during the day, when the Sun is above the horizon (McNamara, 1991).

2.5.1 Layers of the ionosphere

The ionosphere consists of four layers during the day, namely D, E, F1 and F2. They occur at different altitudes due to photoionisation. At night the recombination wins over photoinisation and the F1 layer combines with the F2 layer to form the F layer, the D

layer disappears and the E layer sometimes remains with the F layer. The F2 layer survives throughout the night and is, therefore, the important layer for HF propagation. Figure 2.2 illustrates the day and night electron density profiles of the ionospheric layers during sunspot maximum (solid line) and sunspot minimum (broken lines).

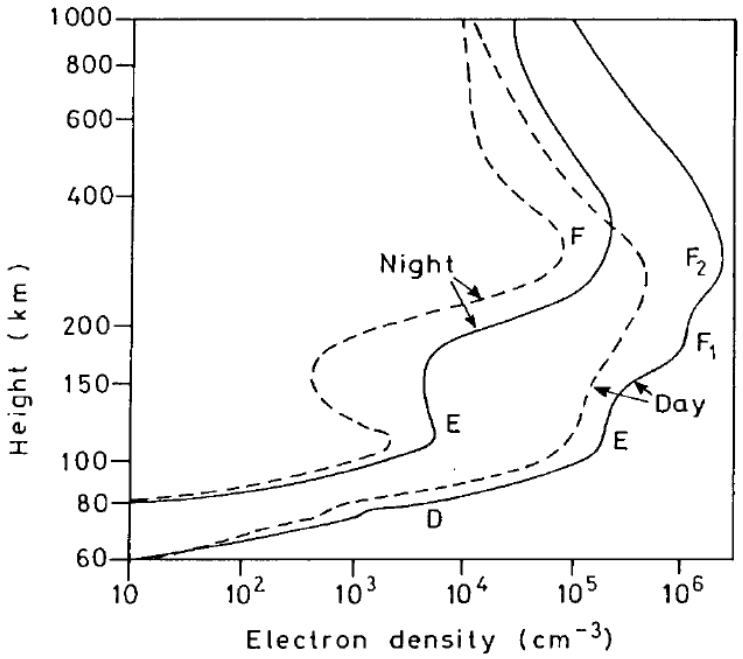

Figure 2.2: The structures and typical vertical profiles of electron density in the mid-latitude ionosphere. Solid and broken lines represent electron density profiles during sunspot maximum and sunspot minimum respectively Credit: Hunsucker and Hargreaves (2003).

2.5.1.1 D layer

The D layer is the lower part of the ionosphere and ranges from about 50 to 90 km above the Earth's surface. It has an electron density of $10^8 - 10^{10}\mathrm{m}^{-3}$. The source of ionisation within this layer is solar Lyman$-\alpha$ radiation which ionises nitric oxide (NO), nitrogen (N), oxygen (O) and the oxygen molecule (O_2) (Thomas, 1996). Cosmic rays play an important role in the ionisation at D layer altitudes, especially during sunspot minimum, when the amount of flux from galactic cosmic rays that reach the Earth's upper atmosphere is higher. This is due to the reduction in shielding effect of the Earth's magnetic field. The loss of electrons in this region is due to the dissociative recombination of the electrons with the positive ions. Due to the high neutral density in the D region the rate of recombination is significantly high as a result of the high collision rate between electrons, molecules and the neutral atoms (Rishbeth and Garriott, 1969; McNamara, 1991). Therefore, the D layer is only present during the day. The D-Layer attenuates the high frequency radio waves due to the high rate of collision between the electrons and the very dense neutral atmosphere at these low altitudes. When

an adequate solar flare occurs on the part of the Sun facing the Earth, some X-rays emitted by the flare will hit the Earth's atmosphere and penetrate down to the D layer. This causes an increase in ionisation by a factor of 10 by a process of photoionisation. Practically, this effect is often disastrous because all the radio waves are absorbed and none left to continue to the receiver, resulting in a phenomenon known as shortwave fadeout. The D-layer has diurnal, seasonal and solar activity variations (McNamara, 1991).

2.5.1.2 E layer

The E layer is the region immediately above the D layer. It extends from about 90 to 150 km above the Earth's surface, and has an electron density of about 5×10^9 m^{-3} at night and about 10^{11} m^{-3} by day (Hunsucker and Hargreaves, 2003). The major sources of ionisation in the E region are low energy X-rays and solar ultraviolet radiation. The major ions are NO^+, O^+ and N^+ (Moldwin, 2008). Ionisation in the E layer increases due to particle precipitation, especially at night when photoionisation is absent.

There are other short-lived sources of ionisation in the E region, such as the complex dynamics which result from the effects of the neutral atmosphere motion, auroral electric fields and meteors entering the upper atmosphere that burn up and impact the surrounding neutral gas with sufficient energy to produce an ionised trail. These sources produce narrow, short-lived regions of dense layers or patches of ionisation at E layer altitudes. This is referred to as sporadic E (Rishbeth and Garriott, 1969). Sporadic E depends on latitude, occurs randomly and may last between a few minutes to several hours. Dense ionisation may cause HF radio waves to be reflected by these trails during long-distance communication (Rishbeth and Garriott, 1969).

2.5.1.3 F layer

The F layer is the uppermost layer of the ionosphere and extends from about 150 to 600 km. The electron density is in the range 10^{11} to about 10^{12} m^3 (Hunsucker and Hargreaves, 2003). During the day it could split into two layers, namely F1 and F2 due to photoionisation. At night recombination takes over, and F1 merges with F2 to form the F layer. The formation of the F layer is due mainly to the ionisation of oxygen atoms by solar EUV radiation (McNamara, 1991).

F1 layer

The F1 layer extends from about 150 to 200 km above the Earth's surface. It is only present during the day and more pronounced during summer than in winter. Ionisation is due to the Lyman continuum of atomic oxygen (O) followed by the nitrogen molecule (N_2).

F2 layer

The F2 layer extends from about 200 to 600 km above the Earth's surface and it peaks at an altitude of about 300 km around local noon. The F2 layer has the highest electron density in the order of 10^6 cm^3, within the ionosphere and the ionisation in this layer is due to EUV solar radiation of atomic oxygen (O). The F2 layer is the most important layer for HF radio communications. During an ionospheric storm the F2 layer could be significantly affected. During severe geomagnetic storms, the critical frequency of the F2 layer may drop below that of the F1 layer (McNamara, 1991).

2.5.2 Ionospheric variations

The various layers of the ionosphere prove that the ionosphere is not stable. It varies with altitude, ranging from the D to F layers. It also varies with time of the day, season, position on the surface of the Earth and solar activity. The variations come with the ionosphere's source of ionisation. Solar ultraviolet and X-ray intensity depend on the position of the Sun in the sky at a particular location on the Earth and the Sun's absolute output (Moldwin, 2008).

2.5.2.1 Diurnal variation

Diurnal variation is the fluctuation that occurs throughout the day. The D, E, and F1 layers only appear during the day and they depend on the zenith angle of the Sun, which is the angle between the line from observer to the position directly overhead and a line from the observer to the Sun. The F2 layer varies throughout the day with a low foF2 in the morning and at night and it peaks at two hours past South African local noon (12 UT) due to the fact that the Earth's atmosphere lags two hours behind the solid Earth's rotation, as illustrated in Figure 2.3 (McNamara, 1991). Figure 2.3 illustrates the variation of foF2 throughout the day. In the early morning hours, just before dawn, and at night foF2 reaches its lowest values due to recombination. When the Sun rises, foF2 increases rapidly as photoionisation starts creating free electrons again (McNamara, 1991). The F2 layer is the most important layer for high frequency communication as it is always present, and the peak of the F2 layer represents the maximum electron density in the ionosphere.

2.5.2.2 Seasonal variation

The nighttime F layer tends to occur at higher altitudes during the summer than during the winter and tends to be thicker. The N_{max}, foF2 and TEC are usually greater in summer than in winter (Davies, 1990; Hunsucker and Hargreaves, 2003). For example, Figure 2.4 shows the seasonal variation of foF2 for 2010 over Grahamstown at 04h00 UT, 10h00 UT

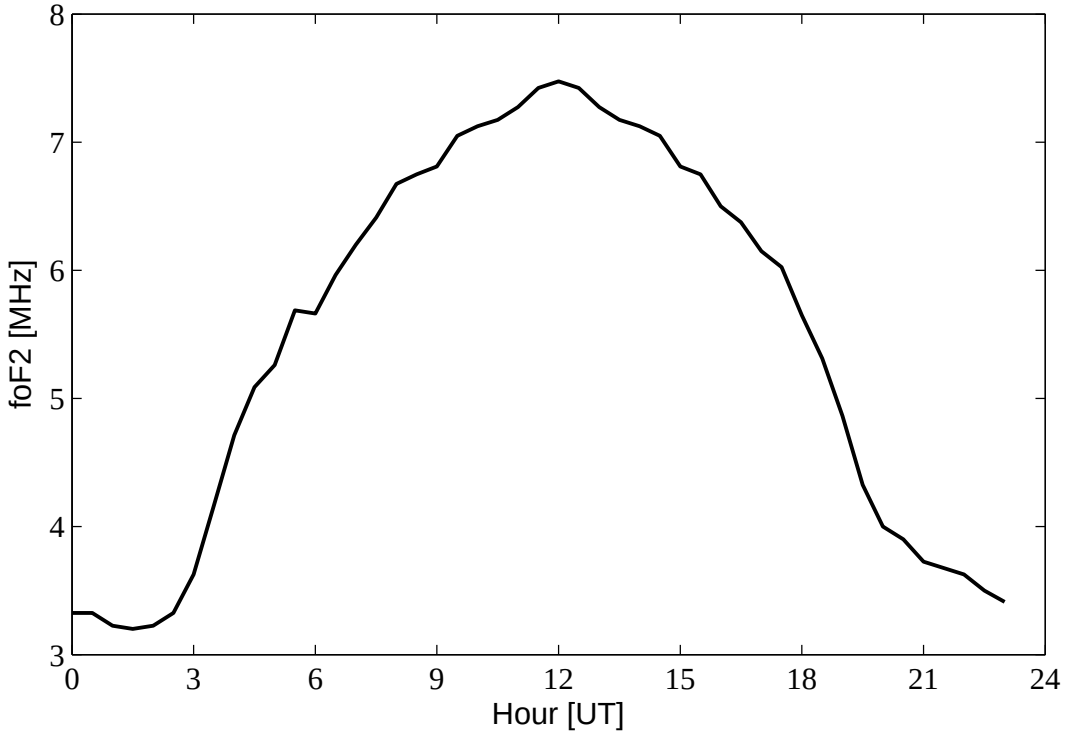

Figure 2.3: An illustration of the diurnal variation of foF2.

and 22h00 UT. At 04h00 UT the foF2 values are low in winter (1 June to 31 August), whereas during summer (1 December to 28/29 February) the foF2 values are higher. Similarly, at 10h00 UT and 22h00 UT during winter foF2 values are low when compared to the summer foF2 values. The foF2 values are greatest during the equinoxes (Autumn (1 March to 31 May) and Spring(1 September to November)). Opperman (2007) notes that at certain times of the year the Sun is vertically above certain geographic locations. At equinox noon (21 March, 23 September) the Sun is vertically above observers at the equator and vertically above observers at the tropics of Capricorn and Cancer on solstice dates (21 December, 21 June). As the vertical illumination from the Sun results in higher ionisation rates, higher electron density concentrations are observed at the locations on these dates than at the other locations.

2.5.2.3 Solar activity variations

The ionosphere is formed through the photoionisation by solar EUV radiation and X-rays. Therefore the behavior of the ionosphere is controlled by the solar activity. The solar activity follows a regular periodic variation over a period of 11 years known as solar cycle. The solar variation over a period of 11 years is measured in terms of sunspots visible on the solar disk, the rate at which flares occur, EUV flux and solar radio flux at 10.7 cm (F10.7 cm). The

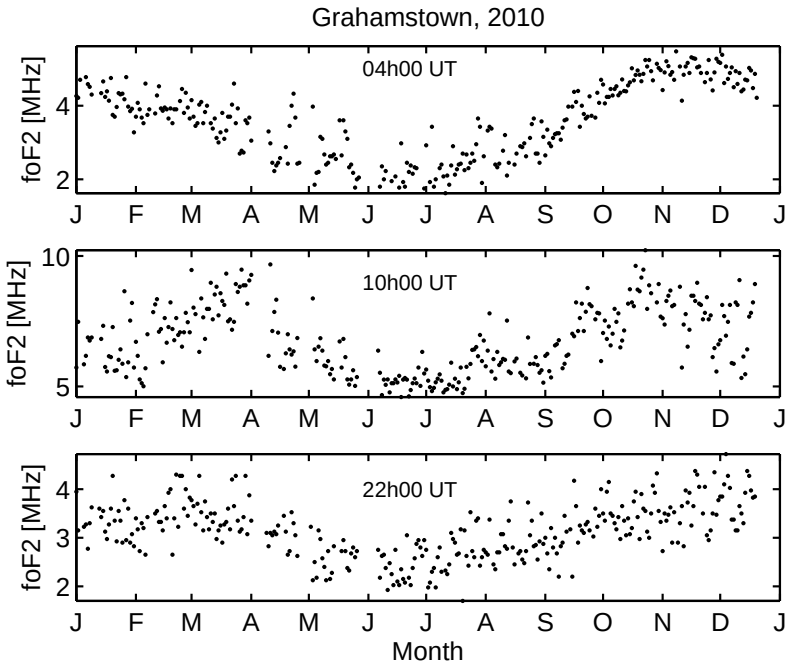

Figure 2.4: Seasonal variation of foF2 over Grahamstown for the year 2010 at 04h00 UT, 10h00 UT and 22h00 UT. J, F, M, A, M, J, J, A, S, O, N, D on the x axis are the first letters of the month.

ionosphere is affected by the variations in the intensity of the ionizing radiations of the X-ray and EUV bands (Hunsucker and Hargreaves, 2003).

During sunspot maximum (which occurs when the solar cycle is at the peak), the ionisation is greater than during the sunspot minimum (which occurs when the solar cycle is at minimum) because the solar radiation is high and hence the electron density in the ionosphere also increases (Davies, 1990). The maxima of E, F1 and F2 regions depends on the solar activity (Hunsucker and Hargreaves, 2003). Figure 2.5 shows the variation of foF2 at 10:00 UT over Grahamstown and sunspot number for 1996 - 2010. This figure shows that the foF2 is highly influenced by solar activity and foF2 follows a synchronous variation with the solar cycle variation. Figure 2.2 also illustrates the variation of electron density profiles during sunspot maximum (dashed lines) and sunspot minimum (broken lines). The electron density profiles are greater during sunspot maximum than during sunspot minimum. The most significant increases in electron density occur at successively higher heights (Davies, 1990).

2.5.2.4 Geomagnetic activity effects

The source of thermal convection at ionospheric altitudes is ultraviolet radiation from the Sun and leads to the movement of ions and electrons across the geomagnetic field. The generated ionospheric current gives rise to a magnetic field in the ionosphere's surroundings and the variations of the generated ionospheric current are later observed as geomagnetic

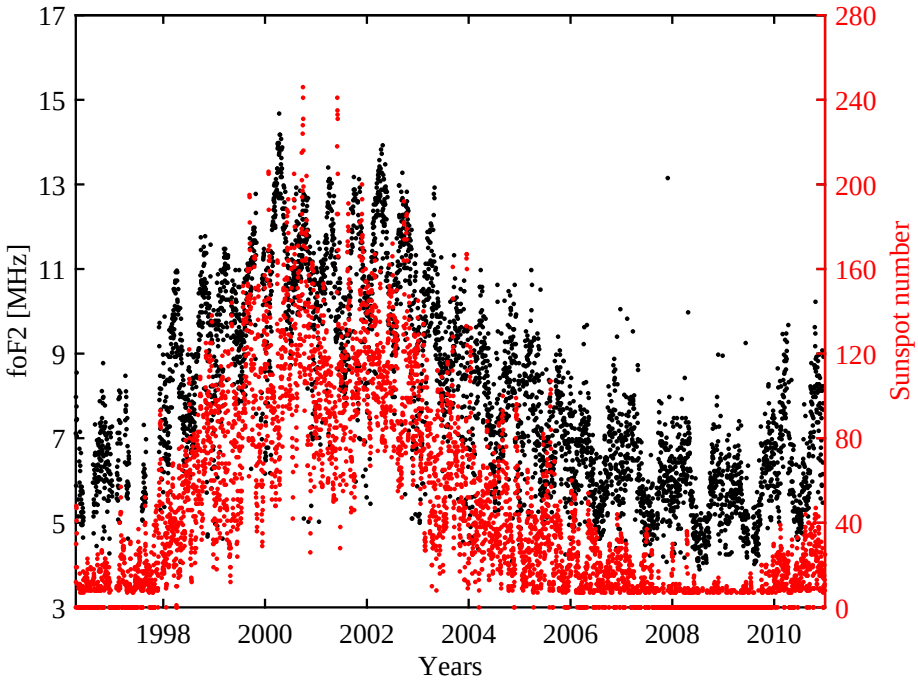

Figure 2.5: The variation of 10:00 UT foF2 values (black) from the Grahamstown station over the period 1996 to 2010. The superimposed are the sunspot number (red)

field fluctuations on the Earth's surface (Ondoh and Marubashi, 2000; Habarulema et al., 2010). During geomagnetic storms the foF2 significantly changes from its normal values. These are termed negative and positive ionospheric storms, corresponding to a decrease or increase in electron density respectively.

2.6 Thermospheric storms

A significant part of the solar wind energy absorbed by the thermosphere during a geospheric storm (an event of strongly enhanced dissipation of solar wind energy in the near-Earth space environment) is dissipated by electric currents and particle precipitation in the polar upper atmosphere. The resultant heating can be so intense that it produces global disturbances in the thermosphere. These are called thermospheric storms (Prölss, 2004).

At high latitudes heating causes expansion of the neutral air which is often rapid during geomagnetic storms. The rapid expansion may cause upwelling in the neutral atmosphere, i.e, the motion of the air through constant pressure surfaces, which results in departures from diffusive equilibrium and increases in the mean molecular mass. Thus, it decreases the atomic oxygen to molecular nitrogen [O/N_2] ratio and molecular oxygen [O_2] densities. Buonsanto (1999) notes that the expansion results in pressure gradients that modify the global thermospheric circulation. The enhanced equatorward winds transport the composition changes

from the high to lower latitudes. These equatorward winds are stronger at night, because they are reinforced by antisunward ion drag due to magnetospheric convection $\mathbf{E} \times \mathbf{B}$ drifts. The latter often take the form of equatorward surges of TADs when the heating events are impulsive. These TADs manifest in the ionosphere as TIDs and increase the electron density at the mid-latitudes (Buonsanto, 1999, and references therein).

Buonsanto (1999) notes that the composition disturbance zone reaches the lower latitudes during summer rather than during winter, when the total wind field includes a prevailing trans-equatorial summer-to-winter flow. This restricts the equatorward motion of the composition changes in winter, while allowing them to reach lower latitudes in summer.

2.7 Ionospheric storms

Ionospheric storms are disturbances in the ionosphere caused by solar activity, such as solar flares and CMEs, and often produce large variations in the particle and electromagnetic radiation on the Earth. They represent an extreme form of space weather with important effects on ground- and space-based technological systems. The ionospheric storms are driven by highly variable solar and magnetospheric energy inputs to the Earth's upper atmosphere (Buonsanto, 1999). During strong geomagnetic storms the electron density of the ionosphere significantly changes from its normal or quiet-time values. The electron density may decrease or increase during geomagnetic storms. The decrease or increase are termed negative or positive ionospheric storm effects respectively. The most studied ionospheric parameter is the Ne of the F2 layer. In this study the foF2 layer was used to study the responses of the ionosphere during geomagnetic storms. The foF2, relates to the electron density of F2 layer by the following expression:

$$\mathrm{Ne} = 1.24 \times 10^{10} (\mathrm{foF2})^2 \tag{2.2}$$

where Ne is the maximum electron density of the F2 layer, measured in e/m^3 and foF2 is measured in MHz (Davies, 1990).

The ionospheric storm effects are determined by a combination of chemical, dynamic, and electrodynamic processes (Rishbeth, 1989; Prölss, 2008; Lu et al., 2008). The most prominent feature of ionospheric storms are the local time and seasonal variations (Prölss, 1995). Geomagnetic storms with nighttime or daytime main phase generally produce negative or positive ionospheric storms respectively (Prölss, 1993*b*, 1995; Gao et al., 2008; Vijaya Lekshmi et al., 2011; Yao et al., 2013).

2.7.1 Negative ionospheric storms effects

Negative ionospheric storms are believed to be caused by changes in the neutral gas composition (Seaton, 1956; Prölss, 1980, 1995, 1997, 2004; Buonsanto, 1999; Zhang et al., 2004; Habarulema et al., 2013b) and the equatorward displacement of the trough region (Prölss et al., 1991; Prölss, 1995). Prölss (1980) showed a direct correlation of magnetic storm-associated changes in atomic oxygen to molecular nitrogen (O/N_2) ratio with the N_{max} ratio of the F layer for the period 17 to 25 February 1973 above 6 mid-latitude stations in the southern hemisphere, including Hermanus (34.4° S, 19.2° E) station, as shown in Figure 2.6.

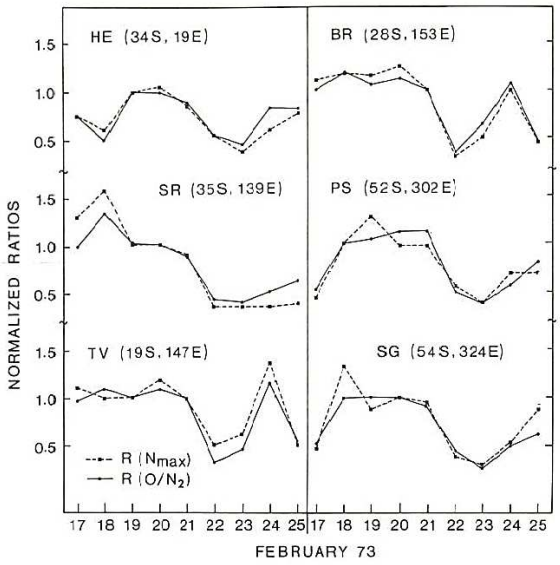

Figure 2.6: Correlation of neutral composition changes with negative ionospheric storm effects. Variations of maximum electron density of F2 layer and the O/N_2 density ratio for the period 17 to 25 February 1973 over the southern hemisphere; HE (Hermanus), SR (Salisbury), TV (Townsville), BR (Brisbane), PS (Port Stanley), and SG (South Georgia) (Prölss, 1980).

A recent study by Habarulema et al. (2013b) showed the depletion of foF2 and TEC during the storm period 6 to 11 November 2004 which correleted well with the decrease in O/N_2 ratio over the Southern Africa region. Katamzi and Habarulema (2014) also showed that the depletion of TEC and foF2 observed during 29 to 31 October 2003 corresponded to a decrease in the O/N_2 ratio over the South African mid-latitudes. During geomagnetic storms, intense Joule and particle heating causes strong upwelling of the atmosphere around the auroral oval, which leads to a variety of dynamic and chemical changes in the atmosphere and increased drag on low Earth orbiting satellites. The strong upwelling of the atmosphere transports oxygen-depleted or nitrogen-rich air from lower down in the thermosphere into the F- region (Mayr and Volland, 1972; Mayer et al., 1978; Prölss, 1980; Chun et al., 2002; Zhang et al.,

2004).

The composition changes during geomagnetic storms expand to the mid-latitudes. The enhancement in molecular nitrogen density and the depletion of oxygen density have important implications for the ionosphere. At F2 layer altitudes the production of ionisation is based on photoionisation of atomic oxygen (Prölss, 1995):

$$\mathrm{O} + \text{Solar radiation}(\lambda \leq 91\text{nm}) \rightarrow O^+ + e^- \tag{2.3}$$

Assuming that the F2 layer is optically thin, the production rate is directly proportional to the density of atomic oxygen $[O]$ i.e.

$$q = J_o[O] \tag{2.4}$$

where J_o is the ionisation frequency of the constituents and q is the rate of production. Thus a decrease in the density of atomic oxygen will decrease the ionisation production rate. The F layer altitudes are primarily due to charge transfer reactions of the type,

$$O^+ + N_2 \quad \underrightarrow{k_1} \quad NO^+ + N \tag{2.5}$$

$$O^+ + O_2 \quad \underrightarrow{k_2} \quad O_2^+ + O \tag{2.6}$$

$$NO^+, O_2^+ + e^- \quad \rightarrow \quad N, O \tag{2.7}$$

where k_1 and k_2 are reaction rate constants. The resulting molecular ions NO^+ and O_2^+ are quickly destroyed by dissociative recombination. The loss rate reduces to $1(\mathrm{N}) = \beta[O^+]$, where β depends on the molecular gases N_2 and O_2.

$$\beta = k_1[N_2] + k_2[O_2] \tag{2.8}$$

An increase in gas will directly increase the loss rate ionisation. The decrease in atomic oxygen density and the increase in molecular nitrogen density combine to reduce the ionisation density at the F layer altitudes. Therefore, an ionosonde station located within the composition disturbance zone will observe negative ionospheric storm effects. The measured composition changes can be used to explain the observed storm effects by calculating the ratio of the disturbed to the undisturbed value of O and N_2

$$R(\mathrm{N}_{max}) \simeq R(O)/R(N_2) = R(O/N_2) \tag{2.9}$$

where N_{max} is the maximum electron density. An increase in molecular gases (N_2) and the decrease in the atomic oxygen (O) density contribute to the decrease in the electron density

(Prölss, 1995).

The negative ionospheric storms have local time as well as seasonal variations. These are the prominent features of the ionospheric storms at mid-latitude. The negative ionospheric storms are usually observed following the geomagnetic storms that occur during the night (Prölss, 1993*b*, 1995; Gao et al., 2008; Vijaya Lekshmi et al., 2011; Yao et al., 2013).

2.7.2 Positive ionospheric storms effects

The origin of positive ionospheric storms is not yet well understood, with several mechanisms having been proposed to explain their origin without arriving at a generally accepted explanation (Prölss, 2008; Ngwira, 2011). For positive ionospheric storm effects the increase in electron density is preceded by a significant increase in the height of the F2 region. Figure

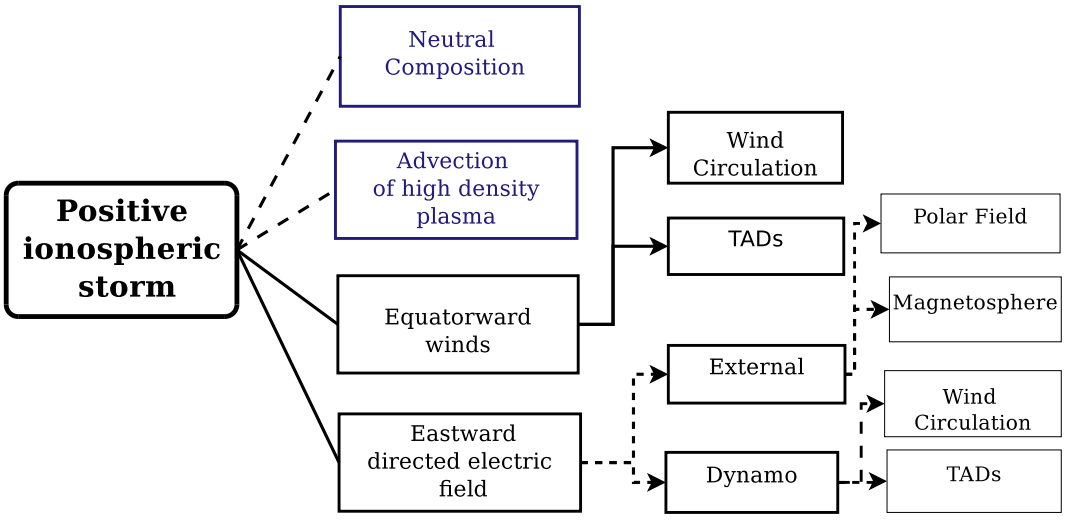

Figure 2.7: Schematic representation for the mechanism contributing to the positive ionospheric storm effect at middle latitude (adopted from, Prölss, 2008).

2.7 illustrates the mechanisms that are usually used to explain the positive ionospheric storm effects. The neutral composition, advection (the transfer of heat or matter by the flow of a fluid horizontally in the atmosphere) of high density plasma, equatorward winds and eastward-directed electric field mechanisms are all important and will contribute to positive ionospheric storm effects. But the neutral composition and advection of high density plasma do not explain the observed increase in layer altitude. However, the equatorward winds and eastward-directed electric field mechanisms are based on an increase in layer altitude (Prölss, 2008).

During equatorward-directed wind the electrons and ions are impacted by a frictional force and the charged particles move freely along and parallel to the geomagnetic field. The field-

aligned component of the frictional force push the ionisation up the inclined magnetic field lines. This motion results in an uplifting of the F2 region. Hence, an increase in layer altitude leads to an increase in electron density (Prölss, 2008).

During the electric field mechanism, the $\mathbf{E} \times \mathbf{B}$ drift causes the height to increase, since it is perpendicular to the inclined geomagnetic field. The $\mathbf{E} \times \mathbf{B}$ drift also leads to an uplifting of the ionosphere. Electrons and ions are the trace constituents of the upper atmosphere, therefore, whatever the neutral atmosphere does during a geomagnetic storm will affect them (Prölss, 2008).

Positive ionospheric storms may be characterized into several classes depending on the duration, local time and latitude. The most observed class of positive storm is the daytime short-duration enhancement of the mid-latitude ionospheric electron density. These are usually attributed to atmospheric disturbances that result from atmospheric gravity waves, that are launched in the high latitudes during storms and travel to mid-latitudes (Jung and Prölss, 1978; Ngwira, 2011).

The TADs are pulse-like perturbations formed by a superposition of gravity waves which propagate at a speed of 600 m/s towards the equator, carrying along equatorward-directed meridional winds. These winds drag the ionisation along the inclined magnetic field lines, thus changing the altitude of the ionisation layer. At mid-latitudes these winds cause an increase in altitude of the F2 layer which in turn will lead to an enhancement in electron density. At F region altitudes the loss rate of ionisation is proportional to the molecular nitrogen and molecular oxygen densities. The loss rate decreases much faster with height than the production rate, which is proportional to the atomic oxygen density. An upward displacement will therefore lead to an overall increase in ionisation density (Prölss, 1995, 1997, 2004).

A second class of positive ionospheric storms is the long-duration positive ionospheric storm effects, which is attributed to two mechanisms: downwelling of neutral atomic oxygen and uplifting of the F layer due to winds. Both mechanisms rely on the large-scale changes in thermospheric circulation caused by heating in the auroral zone.

The downwelling of neutral atomic oxygen mechanism: The altered thermospheric circulation causes downwelling of the neutral species through constant pressure surfaces at low mid-latitude equatorwards of the composition disturbance zone, increasing the density of the oxygen relative to molecular nitrogen (N_2) and molecular oxygen (O_2). This will result in an increasing of the electron density of the F layer (Buonsanto, 1999).

The uplifting of the F layer due to winds mechanism: The long-duration positive ionospheric storm effects occur when the enhanced equatorward winds lift the ionisation to greater heights at a time when production is still occurring. This mechanism works best during the daytime, while the increase in oxygen density causes positive storms at night (Buonsanto, 1999).

A physical mechanism of positive ionospheric storms at low and mid-latitudes reveals that while the eastward PPEF reduces the ionospheric density, the mechanical effects of the equatorward wind increase the density (Balan et al., 2010). Hence, the mechanical effects of the equatorward wind therefore accumulate the plasma at altitudes near and above the ionospheric peak. They accumulate the plasma by increasing the altitude of the ionosphere and reducing the downward diffusion of plasma along the geomagnetic field lines.

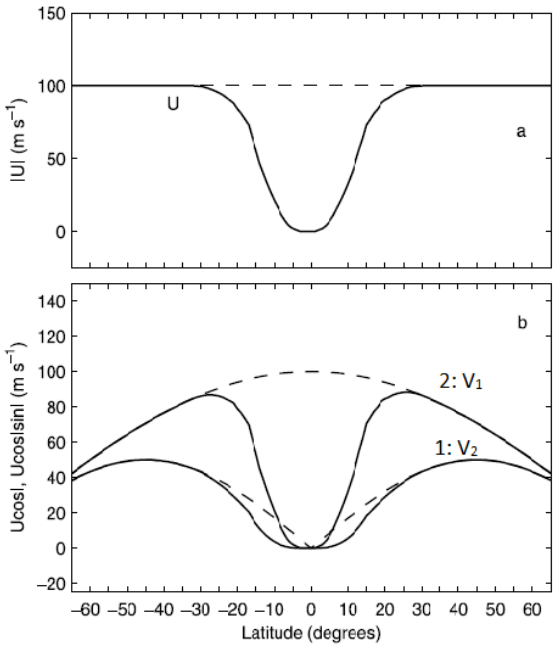

Figure 2.8: Latitude variations of the magnitudes of typical (solid line) and extreme (dashed line) magnetic meridional equatorward neutral wind (U). The direction of wind is opposite in North and South. (b) (1) Latitude variations of V_2 and the increase in the ionospheric peak (Δh) and (2) the component V_1 of U upward along the field lines that reduces the downward diffusion velocity plasma ($V_{\|}$ along the field lines) (Balan et al., 2010)

The motion of the ions maintained by the meridional neutral wind is dependent on the dip angle denoted by, "I", of the geomagnetic field. The equatorward wind (with velocity U) drives the ionosphere up the field lines (with velocity V1)

$$V_1 = U\cos(I) \tag{2.10}$$

The vertical component of the ion velocity V_2 which raises the ionosphere to the altitude of reduced chemical loss and hence accumulates plasma, is given by:

$$V_2 = U\cos(I)\sin(I) \tag{2.11}$$

The ionosphere peaks rise vertically by

$$\Delta h \approx (H/D)U\cos(I)\sin(I) \tag{2.12}$$

where H is the height of the F2-layer peak and D is the diffusion coefficient. The rise can maximize at ($\pm 45^\circ$). Both Grahamstown (-42° magnetic latitude) and Madimbo(-33° magnetic latitude) stations are located within these latitudes and the downward plasma velocity along the field line, due to diffusion, is

$$V_\parallel = -(D_p/n)(dn/dh + n/H_p)\sin I \tag{2.13}$$

where D_p is diffusion coefficient, n is the plasma density and H_p is the plasma scale height. The upward wind velocity V_1 reduces the downward diffusion velocity and hence turns the plasma flux vectors towards the equator and accumulates the plasma. This effect can maximize at low-middle to equatorial latitudes, as shown by curve 2 in Figure 2.8(b) (Miller et al., 1989; Balan et al., 2010).

The accumulated plasma centres around those latitudes where the two mechanical effects optimize. As illustrated by Figure 2.8(b) curves 1 and 2, the two effects optimize around $\pm 30^\circ$ latitude for typical to extreme variations of the equatorward wind. However, V_1 and V_2 cannot be added for vector considerations (Balan et al., 2010).

The mechanical effects of the equatorward wind can therefore produce positive ionospheric storms by accumulating the plasma at altitudes near and above the ionospheric peak centered around $\pm 30^\circ$ latitude. The PPEF shifts the equatorial ionisation anomaly (EIA) crest to about $\pm 30^\circ$ latitude (Balan et al., 2010).

2.7.3 Local time and seasonal variations of the ionospheric storms

Local time and seasonal variations belong to the more prominent features of ionospheric storms (Prölss, 1993*b*, 1995, 2008). The first publication about ionospheric storm effects due to local time variation was given by Kirby et al. (1936) who stated that severe magnetic storms that begin during the daytime may show little variation with radio data (referring to negative storm effects), while a severe magnetic disturbance before sunrise is accompanied by

disturbed radio conditions during the entire day (Prölss, 1993*b*). Ionospheric storms observed at mid-latitude showed a strong dependence on local time (Prölss, 1980, 1993*b*, 1995; Gao et al., 2008; Vijaya Lekshmi et al., 2011; Yao et al., 2013). Most negative ionospheric storms follow the magnetic activity that occurs during the night to early morning local time, whereas the positive ionospheric storm effects follow magnetic activity that occurs in the daytime as well as night local time (Prölss, 1980, 1993*b*, 1995; Gao et al., 2008; Vijaya Lekshmi et al., 2011).

Occurrence of positive or negative ionospheric storm effects indicates seasonal dependence. During summer, negative ionospheric storms occur most frequently at mid-latitude, while during winter they are restricted to higher latitude regions. This is because during summer the composition disturbance zone extends further equatorward by about 20° on average, than during winter (Prölss, 1995). It is believed that the seasonal variations arise from the interaction between seasonal and storm-induced winds. During summer seasonal and storm-induced winds support each other, and during winter they are out of phase. This explains the gradual rise of N_2/O disturbance in the summer hemisphere and the steep rise in the winter hemisphere (Prölss, 1995).

On the other hand positive ionospheric storm effects at mid-latitude are observed mainly during winter. This is due to the limited extent of the composition disturbance zone during winter. Therefore, a much larger proportion of the mid-latitude region is exposed only to wind perturbations. The winter ionosphere may be sensitive to wind perturbations due to its lower altitude during this season (Prölss, 1995).

2.8 Summary

Important aspect of the Sun, solar wind, the solar activity, sunspot, solar flare, coronal mass ejections, and the magnetosphere were discussed. An overview was given of the ionosphere and the mechanisms that lead to positive and negative ionospheric storms. Local time and season are the most prominent features of ionospheric storms. This is due to the limited extent of the composition disturbance zone during winter hence the increased observation of positive ionospheric storms.

Chapter 3

Ionospheric parameters relevant to the study and their data sources

3.1 Introduction

This chapter discusses the data sources used and measurements made in this study. This includes the Dst index, which is the most commonly used index in research on the magnetosphere. It is a measure of magnetic activity. Ionosonde-observed foF2 and GPS TEC observations provide the necessary information to understand the various processes occurring in the ionosphere. The F2 layer is the most important layer of the ionosphere, particularly for HF radio communication. The GPS TEC parameter is also used to study the ionospheric response during geomagnetic storms. For these reasons, these parameters, and their measurement are described as background material for this research.

3.1.1 Geomagnetic storms

A geomagnetic storm is a depression in the horizontal component of the Earth's magnetic field which normally lasts for several hours to several days. The depression in the horizontal component is due to the ring current flowing westward in the magnetosphere. It can be monitored by the Dst index which is expressed in nT, and is based on the average component of the Earth's magnetic field, measured hourly at four near-equatorial geomagnetic stations, namely San Juan, Honolulu, Kakioka and Hermanus. The coordinates of the geomagnetic stations are shown in Table 3.1.

The Dst index only describes the zonally average disturbance and not its local dependence. The Dst index is given by

$$Dst = \frac{1}{N}\sum_{n=1}^{N}\frac{H - H_q}{cos\phi} \tag{3.1}$$

Table 3.1: Coordinates of the the geomagnetic stations were taken from http://wdc.kugi.kyoto − u.ac.jp/dstdir/dst2/onDstindex.html.

	Geographic		Geomagnetic
Observatory	Longitude	Latitude	Dipole latitude
Hermanus	19.22°	-34.40°	-33.3°
Kakioka	140.18°	36.23°	26.0°
Honolulu	201.98°	21.32°	21.1°
San Juan	293.85°	18.01°	29.9°

where H and H_q are the horizontal components of the magnetic field disturbance at a given station and over the quietest days, N is the total number of stations and ϕ is the station latitude. The $cos\phi$ factor normalizes the magnetic disturbances at different latitudes to the values at the equator (Kamide and Malsev, 2007).

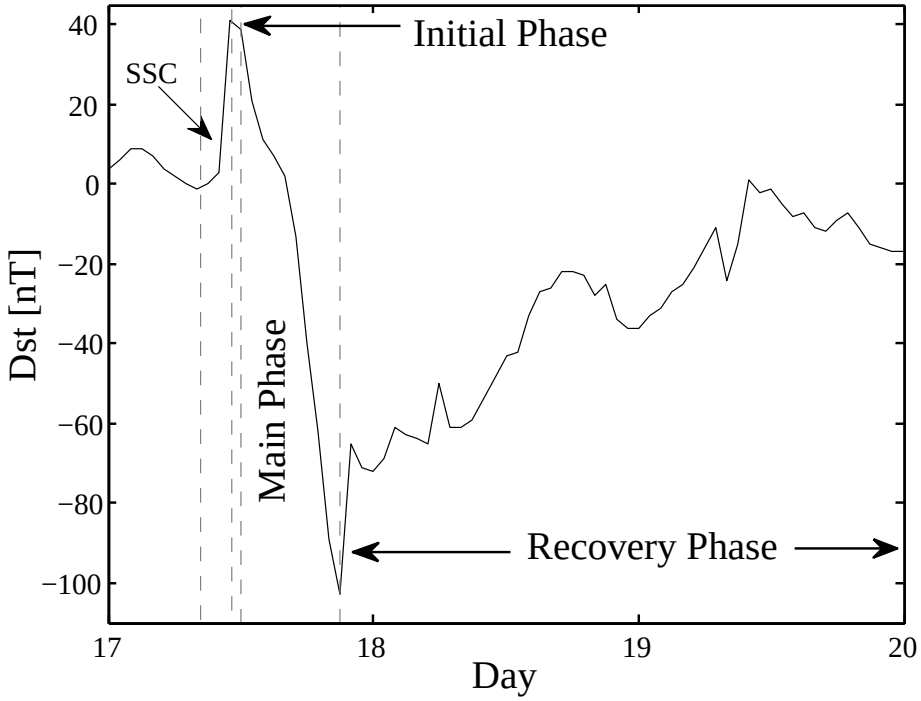

Figure 3.1: An example of a geomagnetic storm from 17 to 19 August 2001 measured by Dst index. The geomagnetic storm is characterized by SSC, Initial phase, Main phase and Recovery phase.

Depending on the solar activity, the assumption is that the magnitude of magnetic storms can be defined by the minimum Dst value. Figure 3.1 is an example of a geomagnetic storm as measured by the Dst index. A geomagnetic storm is characterized by three phases, namely initial phase, main phase and recovery phase.

- **Sudden storm commencement:** SSC is a signature of the changes in a magnetic

storm which may begin either gradually or with an abrupt change, caused by the solar wind shock hitting the Earth's magnetopause and compressing the magnetic field (Davies, 1990). There are storms without a sudden commencement signature. A shock wave hitting the magnetopause does not necessarily lead to storm development. When it is not followed by a storm phase, it can also lead to positive deviation in the magnetograms called a sudden impulse (Koskinen, 2011).

- **Initial phase:** The initial phase begins after the SSC. The initial phase starts when Dst index is positive and relatively steady, as illustrated in Figure 3.1. It can last only for a few minutes or can be persistent for several hours, depending on the structure of the solar wind driver. If the IMF in the sheath region between the ejecta and the shock is southward, the initial phase may be very short and the main phase commences as soon as the energy transfer into the ring current and to the tail current has become strong enough. On the other hand, if the IMF is northward, the main phase will not begin until a southward field of the ejecta increases the reconnection on the dayside magnetopause. Therefore, if there is no southward IMF within the part of the ICME interacting with the magnetosphere, no regular global geomagnetic storm can be expected, except if the event is followed by a fast and long-duration solar wind and with an IMF southward component capable of driving a storm on its own (Koskinen, 2011).

- **Main phase:** The main phase begins when the horizontal component at the equator decreases below the pre-storm value and ends when the Dst reaches its maximum negative value, as shown in Figure 3.1. The field depression during the main phase is produced by an enhancement of the magnetospheric ring current (Davies, 1990; Kamide and Malsev, 2007).

- **Recovery phase:** The recovery phase starts to return to the quiet time values because of the decay of the ring current. The ring current decay is because of the loss processes as charge exchange collisions with neutral hydrogen atoms extracts energy out of the energetic particles. What the process does is to generate an energetic neutral particle, which is not bound anymore by the magnetic field, and low energy ion. Plasma turbulence can cause pitch angle diffusion, and this process brings energetic particles into the loss cone such that they are subsequently lost in the atmosphere (Otto, 2005).

There are other indices for the measurements of the strength or degree of geomagnetic storms, such as the K, K_p, a_p, A_p and AE indices. The K index quantifies disturbances in the horizontal component of the Earth's magnetic field with an integer ranging from 0 to 9. The K_p (planetary K) index is designed to give a global measure of geomagnetic activity. Both K and K_p indices are determined after the end of each three hourly interval. The a_p

(geomagnetic planetary amplitude) index is linear and is equivalent to the K_p index. The A_p index is the average of the eight a_p indices. The AE (Auroral Electrojet) index measures the current flowing in the auroral zone, and it is derived from data obtained at the stations located in longitude near the auroral zone (Davies, 1990). This project used Dst data for storm identification, which was downloaded from the website of the World Data Center (http//wdc.kugi.kyoto-u.ac. jp/ dstae/index.html).

3.2 Ionosonde data

An ionosonde is the most accurate bottomside ionospheric measurement sounder in use. An ionosonde is a HF radar that operates in the frequency band 0.5 to 30 MHZ, and sounds the bottomside (up to the maximum electron density) ionosphere. Ionosondes have been used extensively in remote sensing for monitoring long-term temporal and spatial variations of the ionosphere and also for scientific research (Davies, 1990). There are two possible modulation methods for use in an ionosonde, i.e. the sweep frequency pulsed method and the chirp method. Each method has its own advantages and disadvantages. The principle of the Chirp technique differs from the pulse-amplitude technique in that the radio signals in the Chirp technique are continuous waves in which the frequency is modulated (Davies, 1990, and reference therein).

3.2.1 Ionospheric sounding measurements

Ionospheric sounding experiments determine the electron density profile between the transmitter and the point of highest density, by varying the probing frequency and measuring the time it takes a radio signal wave to travel from the transmitter to the reflection point and back.

Figure 3.2 demonstrates the propagation of radio signal waves through the ionosphere. A radio signal wave transmitted by the transmitter L on the Earth surface enters the ionosphere at point M and is refracted by the electron density at a higher altitude. In the figure, i is the angle of incidence at point M and r is the angle of refraction at point N. The refraction angle at point 0 is 90°. The radio signal wave returns from its maximum height, passes through the ionosphere at P and goes back to the Earth surface to a receiver at Q.

For a radio signal wave of frequency f propagating through the ionosphere, the refractive

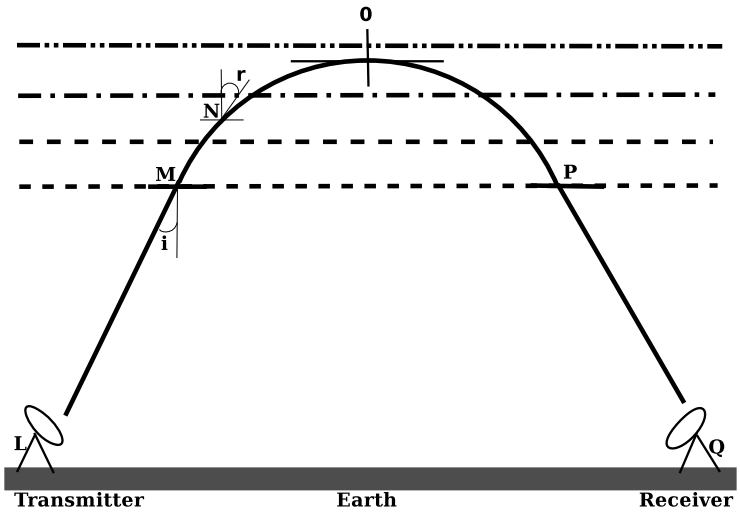

Figure 3.2: A schematic representation of the propagation of radio waves through the ionosphere along the path LMNPQ (adopted from White, 1970).

index can be derived from the Appleton-Hartree equation which is given by:

$$\mu^2 = 1 - \frac{4\pi N_e e^2}{M_e \omega^2} \tag{3.2}$$

where N_e is the electron density measured in electrons/m^3, e is the electron charge equal to -1.602×10^{-19} C, M_e is mass of electron equal to $9.11 \times 10^{-30} kg$ and $\omega = 2\pi f$, where f is radio signal wave frequency (Hz).

μ_M is the refractive index within the ionosphere at M, and at N is μ_N, as illustrated in Figure 3.2. As the wave penetrates the layers, the electron density increases and the wave normal changes according to Snell's law:

$$\mu_M \sin i = \mu_N \sin r. \tag{3.3}$$

At point O at the top of the trajectory in Figure 3.2, the angle r = 90 °. This implies that sin r = sin 90 = 1, then $\mu_0 =$ sin i. For the radio wave signal that does not reach the ionosphere, the inclination angle ($i = 0$) and $\mu_0 = 0$. setting $\mu^2 = 0$ in Equation 3.2 and letting $\omega_0 = 2\pi f_0$ gives

$$f_o = \sqrt{\frac{N_e e^2}{\pi m e}} \tag{3.4}$$

which is the cutoff frequency or critical frequency. Every frequency less than f_o is reflected and will eventually return to Earth, however, the higher frequencies penetrate the ionosphere

and go out into space. Therefore, the maximum electron density at the maximum height is

$$N_e(max) = \frac{\pi m_e f_0^2}{e^2} = 1.24 \times 10^{10} f_0^2 \tag{3.5}$$

This implies that electron density N_e is directly proportional to the square of the critical frequency f_0. The virtual height is related to the time of flight t and the refractive index as follows:

$$h' = \frac{1}{2}ct = \int_0^{h_r} \frac{dh}{u} = \int_0^{h_r} \mu' dh \tag{3.6}$$

where c is the speed of light, u is the group speed and h_r is the real height of reflection (Davies, 1990). A range of radio frequencies are swept to cover the entire range of electron densities, a virtual height versus frequency graph called an ionogram is obtained, samples of which are shown in Figure 3.3 (White, 1970).

3.2.2 Ionograms and their interpretation

The Earth's magnetic field produces ordinary and extraordinary rays. Figure 3.3 gives samples of a daytime (a) and a nighttime (b) ionogram observed at the Grahamstown $(33.3°S, 26.5°E)$ station. The ionograms display two traces of the radio signal waves for each layer of the ionosphere. The ordinary (O) and extraordinary (X) waves which are shown in red and green respectively. The overplotted black curves are the generated electron density profiles. The vertical asymptotes for O and X traces represent the critical frequencies foF2 and fxF2 respectively, and are separated by approximately half the gyrofrequency, f_{ce} (McNamara, 1991).

In order to understand and interpret radio signals propagating through and reflected by the ionosphere to the receiver on Earth, it is important to first understand the radio refractive index of the ionosphere. Neglecting the influence of positive and negative ions on wave propagation, two frequencies can be defined:

$$\text{Plasma frequency } : (2\pi f_{be})^2 = \omega_{be}^2 = N_e e^2/m_e\epsilon_0 \tag{3.7}$$

$$\text{Gyro frequency } : 2\pi f_{ce} = \omega_{ce} = \mathbf{B}e/m_e \tag{3.8}$$

where N_e denotes the concentration of free electrons, m_e is the mass of the electron, e is electron charge, ϵ_0 is the electric permitivity of free space, ω is the angular frequency and

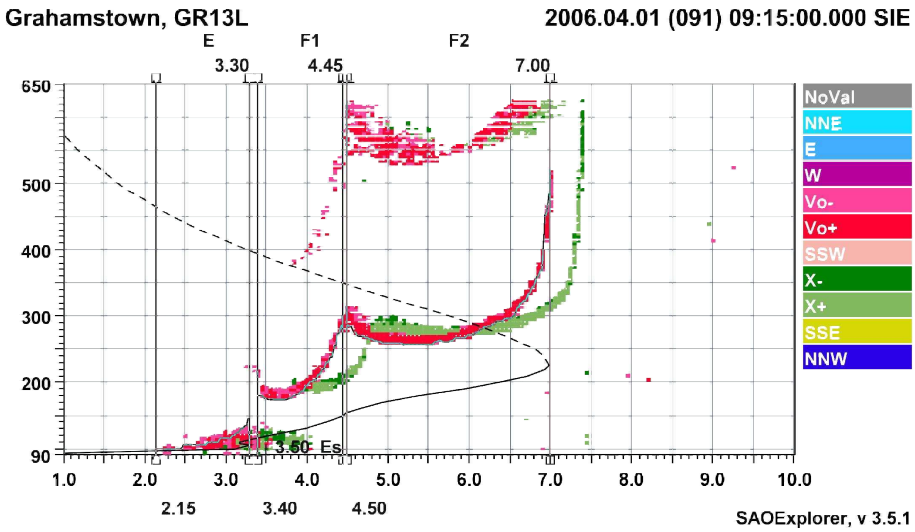

(a) Daytime ionogram

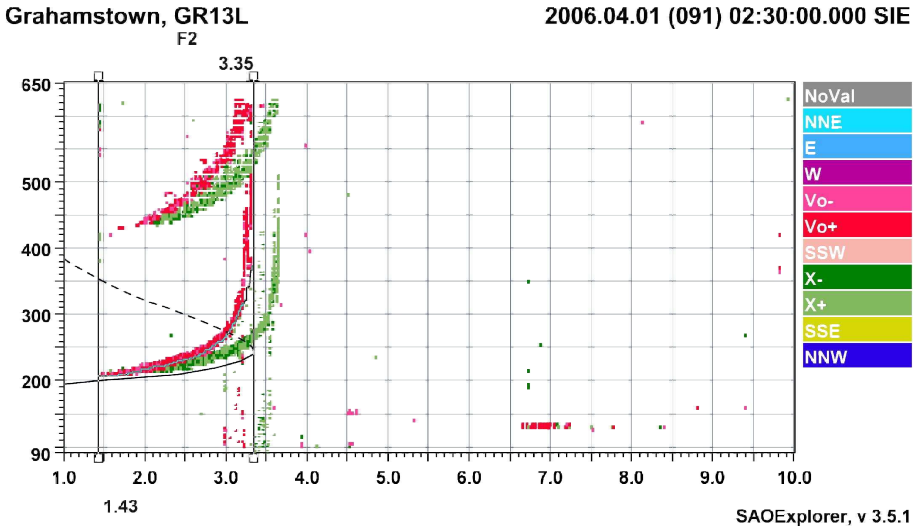

(b) Nighttime ionogram

Figure 3.3: A sample of (a) daytime and (b) nighttime ionograms for Grahamstown $(33.3°S, 26.5°E)$ ionosonde station on the 01 April 2006.

B is the geomagnetic field flux density (Rishbeth and Garriott, 1969; Davies, 1990). Now, let θ be the angle between the wave normal and the direction of magnetic field, therefore, $Y_L = Y cos\theta$, and $Y_T = Y sin\theta$, where the two subscripts L and T refer to the longitudinal and transverse components of the imposed magnetic field. Hence, the magnetoionic parameters can be expressed as

$$X = N_e e^2/\epsilon_0 m_e \omega^2 = \omega_{be}^2/\omega^2,\ Y_L = e\mathbf{B}_L/m_e\omega = \omega_{ce}/\omega,\ Y_T = e\mathbf{B}_T/m_e\omega \text{ and } Z = \nu/\omega \quad (3.9)$$

For the negligible collision frequency in the F region, the case $Z \approx 0$ (Rishbeth and Garriott, 1969; Davies, 1990), the refractive index μ can be expressed in terms of the Appleton-Hatree

formula as:

$$\mu^2 = 1 - \frac{X(1-X)}{(1-X) - \frac{1}{2}Y_T^2 \pm \left[\frac{1}{4}Y_T^4 + (1-X)^2 Y_L^2\right]^{\frac{1}{2}}} \tag{3.10}$$

The positive (+) sign and negative (-) sign refer to the ordinary and extraordinary waves respectively. For the horizontally stratified ionosphere, a vertical incident wave is reflected at a level of $\mu^2 = 0$. This occurs at $X = 1$ for the ordinary wave, which is the same as having no magnetic field. The reflections occur at the level where $X = 1 - Y$ if $Y < 1 (f > f_{ce})$ and where $X = 1 + Y$ if $Y > 1 (f < f_{ce})$ for the extraordinary wave (Rishbeth and Garriott, 1969).

For a normal wave propagating parallel to the magnetic field $\theta = 0$, then $Y_L = Y$ and $Y_T = 0$ and the refractive index μ can be easily simplified from equation 3.10. Again for a normal wave propagating perpendicularly to the magnetic field, the quasi-transverse approximation ($Y_T^4 \gg 4(1-X)^2 Y_L^2$) holds both for $\theta = 90$ with nearly all values of X and the ordinary wave with $X \approx 1$, when $Y << 1$, at nearly all values of θ. Therefore, at $X = 1$ and $\theta = 90$ and at very high frequency the quasi-longitudinal approximation ($Y_T^4 \ll 4(1-X)^2 Y_L^2$) is useful and the refractive index is now expressed as

$$\mu^2 = 1 - \frac{X}{1 \pm Y_L} \tag{3.11}$$

The ordinary and extraordinary wave modes are elliptically polarized. Hence, any plane polarized wave propagating through the ionosphere may be considered the sum of the extraordinary and ordinary components. The plane of polarization continues to rotate along the wave path because the ordinary and extraordinary waves have different phase velocities (Rishbeth and Garriott, 1969; Davies, 1990).

The relationship between the ordinary (O) and extraordinary (X) wave critical frequencies are found from the reflection conditions, $X = 1 + Y$, $X = 1$, and $X = 1 - Y$ (Davies, 1990). As already mentioned, the vertical asymptotes for foF2 and fxF2 are separated by approximately half the gyrofrequency f_{ce} (McNamara, 1991). The O and X waves are reflected at the same height and they are related by the following expression:

$$fo^2 = fx(fx - f_{ce}) = (fx)^2 - fx f_{ce} \tag{3.12}$$
$$\therefore f_{ce} = \frac{f_x^2 - fo^2}{f_x}$$

Hence, if $f_x \gg f_{ce}$ then,

$$fx \cong \frac{f_{ce} + 2fo}{2} \cong fo + \frac{f_{ce}}{2} \tag{3.13}$$

The above formula is important in the interpretation of an ionogram. It differentiates the critical frequency of the O and X ray penetration of a particular layer and vice versa (McNamara, 1991).
The ionosonde data used in this study was obtained from ionosonde stations Grahamstown $(33.3°S, 26.5°E)$ and Madimbo $(22.4°S, 30.9°E)$ operated by the SANSA.

3.3 Global positioning system data

The GPS is a satellite-based radio navigation system. The GPS operational constellation comprises 24 satellites which orbit the Earth in six orbital planes in 11 h 58 m with an inclination angle of 55° relative to the equatorial plane and a radius of approximately 20,200 km. The six orbital planes are separated by 60° in the equatorial plane. The satellites are located such that a user anywhere in the world has a direct line of sight to at least four satellites at any time. The satellites emit coded radio signals that a GPS receiver decodes to determine important system parameters. The satellites are operated and maintained by the USDoD. GPS was initially intended for military applications, but in the 1980s the government made the system available for civilian use such as road and rail transport, aviation, shipping, science, security, surveying, mapping, Geophysics, telecommunications, etc (Farrell and Barth, 1998; Misra and Enge, 2006).

GPS consists of three main segments, namely Space, Control and User.

Space segment
The space segment consists of 24 satellites orbiting in six orbital planes with four satellites in each plane, as already mentioned.

Control segment
The control segment consists of a global network of ground facilities that track and monitor satellite transmission, perform analysis and send commands and data to the GPS operational constellation. The current operational control segment includes the *master control station, ground-based Antenna,* and *monitor stations. The master control station* generates and uploads navigation messages and ensures the health and accuracy of the satellite constellation. The master control station receives the navigation information from the monitor station and uses it to compute the precise locations of the GPS satellites in space, and then uploads this

data to the satellites (Gps.gov, 2014).

Monitor stations track the GPS satellites as they pass overhead and channel their observations back to the master control station. They also collect atmospheric data, range/carrier measurements, and navigation signals. There are sixteen monitoring stations throughout the world, namely 10 stations of the National Geospatial-intelligence Agency (NGA) and six of the United States Air Force (Gps.gov, 2014).

The *ground antennas* communicate with the GPS satellites for control and command purposes. The antennas support the S-band communication protocol. This links or sends navigation data uploads and processor program loads and collect telemetry. The ground antennas are also responsible for normal command transmissions to the satellites (Gps.gov, 2014).

User segment The user segments consist of antennas and receiver processors that measure and decode the satellite transmissions to provide positioning, velocity and precise timing information to the user (Farrell and Barth, 1998).

3.3.1 GPS signal

Each GPS satellite continuously broadcasts radio signals using two L-band frequencies which are referred to as L1 (Link 1) and L2 (Link 2). The L-band covers frequencies between 1 GHz and 2 GHz. Therefore the centre frequency between L1 and L2 is

$$\text{L1: } f_{L1} = 1575.42 \text{ MHz and L2: } f_{L2} = 1227.60 \text{ MHz.}$$

The coarse/acquisition code is modulated on the L1 carrier phase. Each satellite has different C/A PRN codes and each PRN code is nearly orthogonal to all other C/A PRN codes. The precise (P) code modulates both L1 and L2. The P-code is a long PRN code. The P-code is encrypted into the Y-code in the AS mode of operation. Only authorized users with the cryptographic keys can use the encrypted Y-code which requires a classified AS module for each receiver channel (Farrell and Barth, 1998).

3.3.2 Total electron content from GPS

The GPS network provides an opportunity to derive the TEC for global and regional ionospheric structures. TEC is the key parameter for describing the ionosphere and is also used to correct ionospheric effects which degrade Global Navigational Satellite System (GNSS) positioning accuracy. The influence of the ionosphere on GNSS measurements depends on GNSS signal frequency and TEC. TEC is the line integral of electron concentration from the GNSS receiver to satellite position. TEC is measured in units of 10^{16} electrons per m^2.

TEC determined from the GPS signals may be used to investigate ionospheric variation. The electron content does not depend on the assumptions related to the Earth's magnetic field and reaches up to a height of 20,000 km (Davies and Hartmann, 1997). Neglecting the assumptions of the magnetic field, where $Y = 0$, Equation 3.10 reduces to:

$$\mu^2 = 1 - X \tag{3.14}$$

At GPS frequencies, the higher order terms may be neglected and the refractive index may be approximated (Parkinson et al., 1996) as:

$$\mu \approx 1 - \frac{1}{2}X \tag{3.15}$$

where

$$\begin{aligned} X = N_e e^2/\epsilon_0 m_e \omega^2 &= \omega_{be}^2/\omega^2 \\ &= \left(\frac{2\pi f_{be}}{2\pi f}\right)^2 = \frac{f_{be}^2}{f^2} \end{aligned} \tag{3.16}$$

therefore,

$$\mu \approx 1 - \frac{1}{2}\frac{f_{be}^2}{f^2} \tag{3.17}$$

but from Equation 3.7 plasma frequency $f_{be}^2 = \frac{N_e e^2}{4\pi^2 m_e \epsilon_0}$, where $\epsilon_0 = 8.854 \times 10^{-12}$ Fm^{-1}. Therefore, plasma frequency becomes:

$$\begin{aligned} f_{be}^2 &= \frac{N_e e^2}{4\pi^2 m_e \epsilon_0} \\ &= \frac{N_e(-1.602 \times 10^{-19} C)^2}{4\pi^2(9.11 \times 10^{-31}\text{ kg})(8.854 \times 10^{-12}\text{ Fm}^-1)} \\ &= 80.594 N_e \end{aligned}$$

substitute f_{be}^2 into Equation 3.17,

$$\begin{aligned} \mu &\approx 1 - \frac{80.594 N_e}{2f^2} \\ \mu &\approx 1 - \frac{40.30 N_e}{f^2} \end{aligned} \tag{3.18}$$

Thus the phase and group refractive index is given by

$$\mu_p = 1 - \frac{40.30 N_e}{f^2} \tag{3.19}$$
$$\mu_g = 1 + \frac{40.30 N_e}{f^2}$$

The group refractive index may be written in terms of the phase refractive index (Kaplan and Hegarty, 2006) as

$$n_g = n_p + f \frac{dn_p}{df} \tag{3.20}$$

where the phase (n_p) and group (n_g) refractive indices are defined by

$$n_p = \frac{c}{\nu_p} \tag{3.21}$$
$$n_g = \frac{c}{\nu_g}$$

f is the signal frequency and ν_p and ν_g are the phase and group velocity respectively. Wave propagation is independent of frequency and the signal phase in a non-dispersive medium, and signal information propagates at the same speed with $\nu_g = \nu_p$ and $n_g = n_p$ (Kaplan and Hegarty, 2006).

3.3.3 Ionospheric effects

The ionosphere is a dispersive medium located at about 50 to 1200 km above the Earth surface. As stated in Chapter 1, the ionosphere consists of free electrons and ions which are formed during an interaction of extreme ultraviolet radiation. These free electrons influence electromagnetic wave propagation, for example the GPS satellite signal. The following series approximates the phase index of refraction in the ionosphere (Hofmann-Wellenhof et al., 1997; Kaplan and Hegarty, 2006):

$$n_p = 1 + \frac{c_2}{f^2} + \frac{c_3}{f^3} + \frac{c_4}{f^4} + ... \tag{3.22}$$

where the coefficients c_1, c_2, c_3 and c_4 are dependent on electron density N_e, but do not depend on frequency. Neglecting higher order terms gives:

$$n_p = 1 + \frac{c_2}{f^2} \tag{3.23}$$

differentiate Equation 3.23 with respect to frequency:

$$\frac{dn_p}{df} = -\frac{2c_2}{f^3} \tag{3.24}$$

substitute Equation 3.23 and Equation 3.24 into Equation 3.20:

$$\begin{aligned} n_g &= 1 + \frac{c_2}{f^2} + f(-\frac{2c_2}{f^3}) \\ &= 1 + \frac{c_2}{f^2} - \frac{2c_2}{f^2} \\ \therefore n_g &= 1 - \frac{c_2}{f^2} \end{aligned} \tag{3.25}$$

The phase and the group indices have opposite signs as can be seen in Equation 3.23 and Equation 3.25. The coefficient c_2 is approximated as $c_2 = -40.3N_e$ [Hz^2]. The rewriting of Equation 3.23 and Equation 3.25 gives the phase and group refractive index, which is similar to Equation 3.19:

$$\begin{aligned} n_p &= 1 - \frac{40.3N_e}{f^2} \\ n_g &= 1 + \frac{40.3N_e}{f^2} \end{aligned} \tag{3.26}$$

Substitution of Equation 3.26 into phase and group velocity in Equation 3.21 gives

$$\begin{aligned} \nu_p &= \frac{c}{1 - \frac{40.3N_e}{f^2}} \\ \nu_g &= \frac{c}{1 + \frac{40.3N_e}{f^2}} \end{aligned} \tag{3.27}$$

$\nu_p > \nu_g$ because the electron density N_e is always positive. Therefore, due to the different velocities, a group delay and a phase advance occur. In the case of GPS code, measurements are delayed and the carrier phases are advanced. Hence, the carrier phase pseudoranges are measured too short and the code pseudoranges are measured too long, compared to the geometric range between the satellite and the receiver. The difference in both measurements is the same (Hofmann-Wellenhof et al., 1997; Kaplan and Hegarty, 2006).

The measured range (s) between the receiver (R) and satellite (S) along the signal path,

according to Fermat's principle (Hofmann-Wellenhof et al., 1997; Kaplan and Hegarty, 2006) is defined by:

$$s = \int n ds \tag{3.28}$$

The geometric range s_0 along the straight line between the satellite and the receiver can be found by setting n = 1

$$s_0 = \int ds_0 \tag{3.29}$$

The ionospheric delay (Δ^{Iono}) is the difference between the geometric range and the measured range and follows from:

$$\Delta^{Iono} = \int n ds - \int ds_0 \tag{3.30}$$

For a phase refractive index n_p, and for a group refractive index (n_g) obtained from Equation 3.23 and Equation 3.25 respectively, the ionospheric delay may be written as follows:

$$\Delta_p^{Iono} = \int \left(1 + \frac{c_2}{f^2}\right) ds - \int ds_0 \tag{3.31}$$

$$\Delta_g^{Iono} = \int \left(1 - \frac{c_2}{f^2}\right) ds - \int ds_0 \tag{3.32}$$

By considering the integration along the path, ds becomes ds_0 and the two equations can be simplified:

$$\Delta_p^{Iono} = \int \frac{c_2}{f^2} ds_0 \tag{3.33}$$

$$\Delta_g^{Iono} = -\int \frac{c_2}{f^2} ds_o$$

Substitute $c_2 = -40.3 N_e$ Hz^2

$$\Delta_p^{Iono} = -\frac{40.3}{f^2} \int N_e ds_0 \tag{3.34}$$

$$\Delta_g^{Iono} = \frac{40.3}{f^2} \int N_e ds_0$$

The electron density along the signal path is referred to as TEC. TEC is defined as:

$$\text{TEC} = \int N_e ds_0 \tag{3.35}$$

substitution of TEC into Equation 3.34 gives

$$\Delta_p^{Iono} = -\frac{40.3}{f^2}\text{TEC} \tag{3.36}$$
$$\Delta_g^{Iono} = \frac{40.3}{f^2}\text{TEC}$$

3.4 Ionospheric shell model

The ionospheric mapping function is one of the approximation to be taken into account when ionospheric delay of radio signals is estimated from GPS data. For the mapping function, the ionosphere is assumed to be located in a shell at altitude (H) which is taken as the F2 peak height hmF2 (see Figure 3.4).

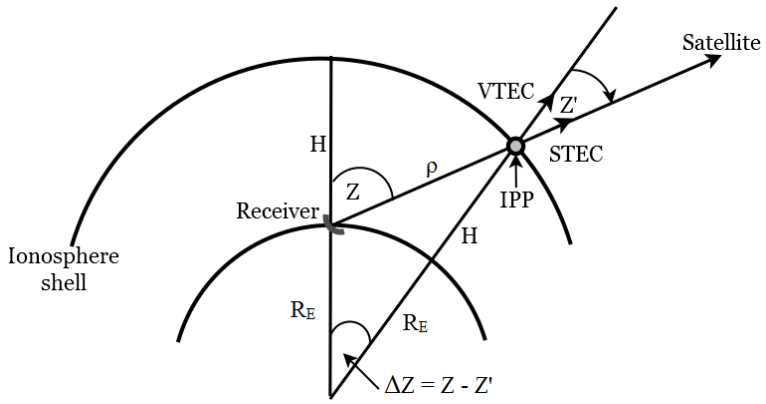

Figure 3.4: Geometry of the Vertical Total Electron Content (VTEC) and Slant Total Electron Content (STEC) mapping function. Ionospheric shell height (H) corresponds to typical F2 peak height, $hmF2 \sim 300 - 500$ km. VTEC is mapped at geographic location of the IPP, distinct from the receiver location (Adopted from Opperman, 2007).

Slant TEC measurements can be converted using the geometry of Figure 3.4, that is,

$$STEC = \frac{VTEC}{cosZ'} \tag{3.37}$$
$$sinZ' = \frac{R_E}{R_E + H} sinZ$$

where, Z and Z' are the zenith angles at the ionospheric pierce point (IPP), R_E is the radius of the Earth and H is the assumed ionospheric shell height as illustrated in Figure 3.4. The STEC is an ionospheric delay at the IPP as observed from the receiver's position. The aim of the mapping function is to allow a geographic conversion of STEC ionospheric delay to VTEC ionospheric delay at the same geographic point. Equation 3.37 is used to convert STEC to VTEC.

At Grahamstown ($33.3^oS, 26.5^oE$) the GPS receiver observations were used to derive TEC with the software developed by Boston College (Seemala and Valladares, 2011) for the period 2006 - 2011. (At Grahamstown ($33.3^oS, 26.5^oE$)) the GPS receiver and ionosonde are co-located)

3.5 Conclusion

This chapter discussed the data sources and measurements used in this study. Background information on geomagnetic storms, including the indices that are used to monitor the horizontal component of the Earth's magnetic field, was given. Measurement capabilities of the ionosonde and GPS were discussed as relevent to the data used for this study. The equation that differentiates the critical frequency of the ordinary and extraordinary rays of a particular layer was derived. The phase and group refractive indices were fully derived for the case when the effects of the magnetic field are negligible and for the case based on the electromagnetic wave propagation. The derivation of ionospheric delay which contains TEC was covered in this chapter.

Chapter 4

Results and discussion

4.1 Introduction

This chapter discusses a statistical analysis of the ionospheric response over the ionosonde stations, Grahamstown (33.3°S, 26.5°E) and Madimbo (22.4°S, 30.9°E), South Africa during geomagnetic storm conditions which occurred during the period 1996 to 2011. Total Electron Content (TEC) derived from Global Positioning System (GPS) data by a dual Frequency receiver and an ionosonde at Grahamstown, was analysed for the storms that occurred during the period 2006 - 2011. This chapter covers the method used to identify the ionospheric response to storm conditions. It explains the responses of the ionosphere during geomagnetic storms and discusses the statistics of the ionospheric storm effects. Furthermore, it illustrates the dependence of the ionospheric storms on Dst intensity, local time and season.

4.2 Data and methods

A geomagnetic storm period was identified by the criterion Dst ≤ -50 nT (Vijaya Lekshmi et al., 2011). Dst data was downloaded from the website of the World Data Center in Kyoto (http//wdc.kugi.kyoto-u.ac.jp/dstae/index.html). A total of 346 geomagnetic storms were identified during the period 1996 to 2011. The geomagnetic storms were classified according to the classes used by Loewe and Prölss (1997), as described in Table 4.1.

Table 4.1: Geomagnetic storms classification (Loewe and Prölss, 1997)

Storm class	**Dst** $[nT]$	**Classification**
1	-50 to -100	moderate
2	-100 to -200	strong
3	-200 to -350	very strong
4	< -350	great

Ionosonde foF2 data for Madimbo (22.4°S, 30.9°E) and Grahamstown (33.3°S, 26.5°E) corresponding to each storm period, were then extracted at 15-minute intervals using the SAO explorer software. For data integrity and accuracy, the ionograms for the analyzed period were manually edited. For Grahamstown (33.3°S, 26.5°E) the co-located GPS receiver observations for the period 2006 to 2011 were used to derive TEC with software developed by Boston College (Seemala and Valladares, 2011). TEC data for this period was later compared with foF2 data to identify the ionospheric response. To obtain near-vertical TEC observations for effective comparisons over the ionosonde stations, only TEC data for satellites with elevation angles greater than 60° were used for the analysis. For both foF2 and TEC data, the measure of disturbance was determined by using the deviations calculated by

$$\Delta X = \frac{X - X_m}{X_m} \times 100\% \tag{4.1}$$

where X_m is the monthly median of the foF2 or TEC during the month when a storm occurred and X represents the time series TEC or foF2 during the storm period. A similar technique was used in related studies (e.g. Gao et al., 2008; Danilov, 2001). In this study the classification of ionospheric response is based on the nature of dominant deviation values of ΔX during quiet periods prior to the geomagnetic storm. The consideration of quiet periods before and after the storm periods, leads to five classes of ionospheric storms, namely positive (P), negative (N), positive followed by negative (PN), negative followed by positive (NP) and not significant (NS) ionospheric storms. Where P is an increase in ΔX, N is a decrease in ΔX, PN is an increase followed by decrease in ΔX, NP is a decrease followed by increase in ΔX and NS is when there is no significant effect on ΔX. There were periods when geomagnetic storms were observed, but no foF2 data was recorded to classify the ionospheric effects. Table 4.2 illustrates the number of geomagnetic storms which occurred from 1996 to 2011 along with the number of storm periods for which foF2 data is not available and therefore no ionospheric response was determined. Due to this paucity of ionospheric data for geomagnetic storms over, in particular, the Madimbo station most of the discussion in the results section is based on Grahamstown (33.3°S, 26.5°E) for which there is much ionosonde data.

Table 4.2: Geomagnetic storms for the period 1996 to 2011 using the Dst ≤ -50 nT as criterion. The number of geomagnetic storms for which there is no foF2 data for Madimbo (22.4°S, 30.9°E) and Grahamstown (33.3°S, 26.5°E) is also shown.

Year	**Total number of geomagnetic storms**	**Storms with no data (Madimbo)**	**Storms with no data (Grahamstown)**
1996	11	11	7
1997	22	22	3
1998	28	28	3
1999	27	27	7
2000	41	33	3
2001	28	13	4
2002	40	26	1
2003	47	6	1
2004	30	7	0
2005	37	26	5
2006	8	1	0
2007	5	0	0
2008	5	1	0
2009	1	1	0
2010	8	5	4
2011	13	0	4

4.3 Results and discussion

4.3.1 The response of foF2 during geomagnetic storms over Grahamstown (33.3°S, 26.5°E)

Figures 4.1, 4.2, 4.3, 4.4 and 4.5 are examples of P, N, PN, NP and NS ionospheric storm effects respectively. These figures also show the variation of Dst, foF2 and its deviation from monthly median values during each storm period.

Figure 4.1 shows that the P ionospheric storm effect was observed from 7 to 10 April 2006 over Grahamstown (33.3°S, 26.5°E). The Dst index shows that the geomagnetic storm occurred on 9 April 2006 with a minimum intensity of -80 nT. The 7^{th} and 8^{th} of April 2006 were quiet days and were compared with the disturbed day (9^{th} April 2006) to check the variation of foF2. The geomagnetic storm that occurred on 9 April 2006 caused the foF2 value to increase, compared to monthly foF2 values. The deviations of foF2 clearly show a significant increase in ΔfoF2 of about 80%. The daytime P ionospheric storm effects in mid-latitude are attributed to the TADs which manifest in the ionosphere as TIDs (Prölss and Jung, 1978; Prölss, 1993*a*,*b*, 1995, 1997, 2004; Ngwira, 2011).

P ionospheric storm effects have been reported for the Southern African region (Ngwira, 2011; Ngwira et al., 2012a; Amabayo et al., 2012; Habarulema et al., 2013b; Katamzi and Habarulema, 2014). All these sources mention storm TIDs as possible sources of electron content enhancement during the geomagnetic storms and hence contribute to the P storm effect. Habarulema et al. (2013a) showed that these storm-induced TIDs were propagating equatorward using TEC data for the storm conditions of 15 May 2005 and 26 September 2011.

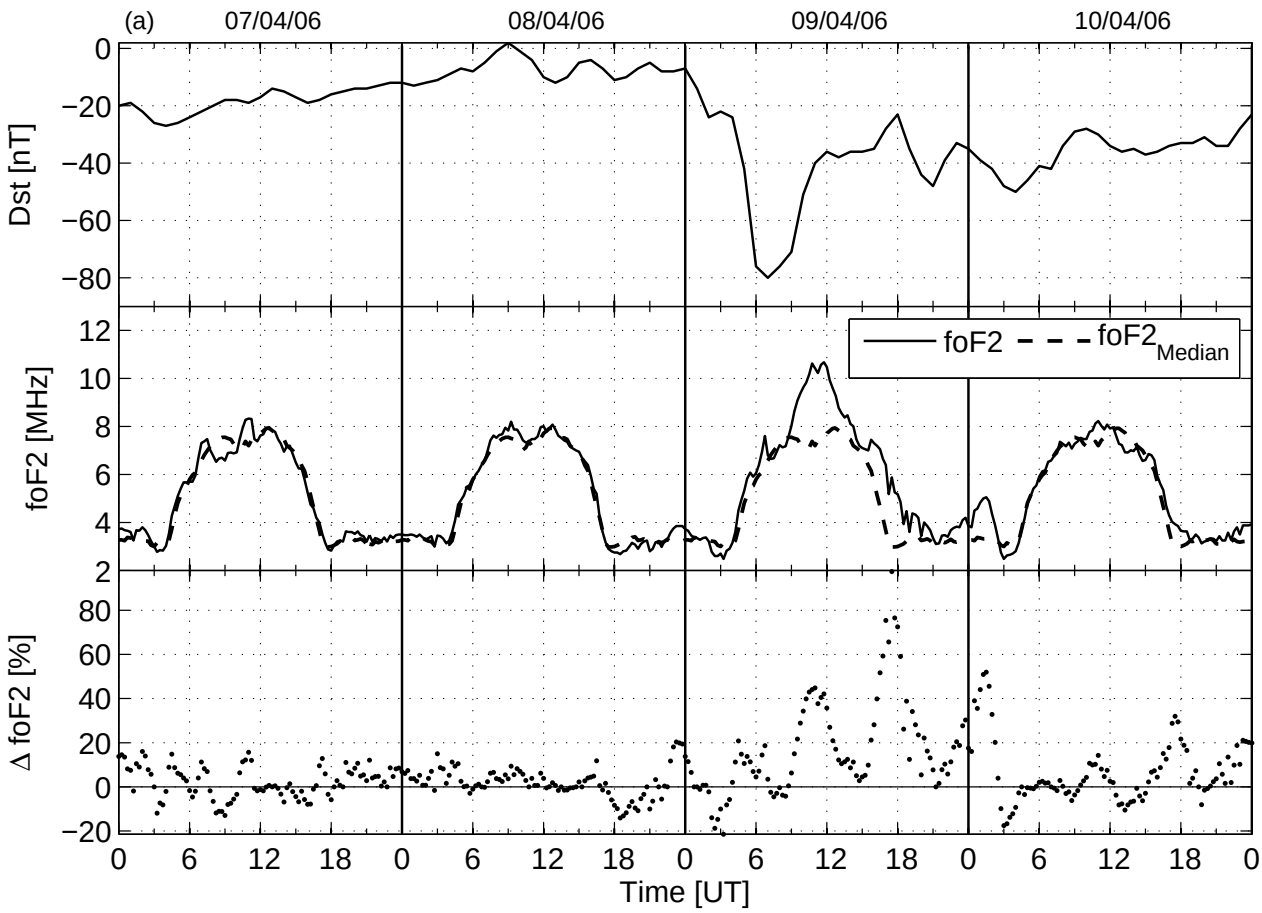

Figure 4.1: An example of P ionospheric storm effects over Grahamstown (33.3°S, 26.5°E)

Figure 4.2 is an example of N ionospheric storm effects for the period 6 to 10 April 2000. The geomagnetic storm occurred on 6 April 2000 with a minimum Dst index of −287 nT. This caused a depletion in foF2 (about 8.65 MHz at the peak) when compared to the monthly median value of foF2 (about 13.82 MHz at the peak) on the next day. The deviations of foF2 clearly show a significant decrease in ΔfoF2 of about −63.62%. The decrease in foF2 could be attributed to neutral composition changes (Jung and Prölss, 1978; Prölss, 1980, 1995, 2004; Zhang et al., 2004; Habarulema et al., 2013b).

N ionospheric storm effects have been reported for the Southern African region (Prölss, 1980; Habarulema et al., 2013b). They were attributed to changes in neutral composition, mainly related to changes in the atomic oxygen to molecular nitrogen (O/N_2) ratio. Prölss (1980) compared the variation of the F layer maximum electron density (N_{max}) and the O/N_2 ratio, using gas analyser measurements over the southern hemisphere, including the Hermanus (34.4°S, 19.2°E) ionosonde station. Habarulema et al. (2013b) also showed, using global maps of the O/N_2 ratio, that the depletion of foF2 and hmF2 were due to the decrease of O/N_2 over Grahamstown (33.3°S, 26.5°E) and Madimbo (22.4°S, 30.9°E) ionosonde stations. However, Adewale et al. (2011) studied the response of the equatorial ionospheric F region

in the African sector to different geomagnetic storms, including the geomagnetic storm of 5 to 10 April 2000. They observed N and P ionospheric storm effects on TEC during the main phase and recovery phase of the geomagnetic storm respectively.

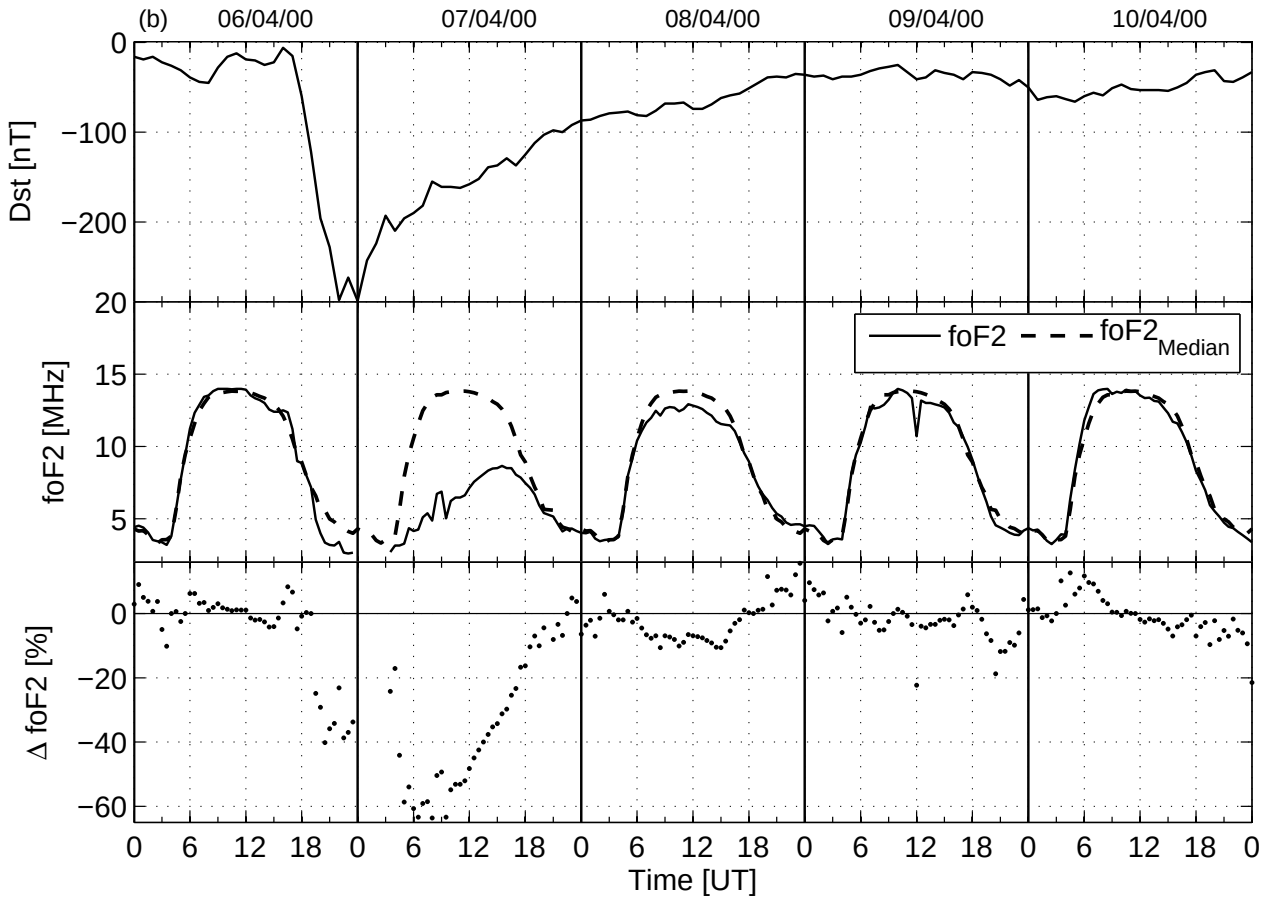

Figure 4.2: An example of N ionospheric storm effects over Grahamstown (33.3°S, 26.5°E)

Figure 4.3 shows an example of a PN ionospheric storm effect for the period 8 to 13 September 2005. The geomagnetic storm, with a minimum Dst index of −70 nT, caused the P ionospheric storm effect on foF2 on 10 September 2005 and a deviation increase of about 36%. After the geomagnetic storm recovered, another geomagnetic storm followed with a minimum Dst index of −147 nT on 11 September 2005, which caused a depletion of foF2 compared to the monthly foF2 values. ΔfoF2 showed a significant decrease of about −48.16%. The increase and decrease in foF2 could be due to the changes in neutral composition. The enhanced O/N_2 ratio causes an increase in foF2 and the decrease in O/N_2 ratio causes the foF2 to decrease (Prölss, 1980; Buonsanto, 1999). Lu et al. (2008) studied a dayside ionospheric P storm phase on the 10 September 2005 over Millstone Hill and Arecibo, driven by neutral winds. Lu et al. (2008) reported that the P storm phase of 10 September 2005 was due to the enhanced meridional neutral wind, rather than the penetration magnetospheric electric field.

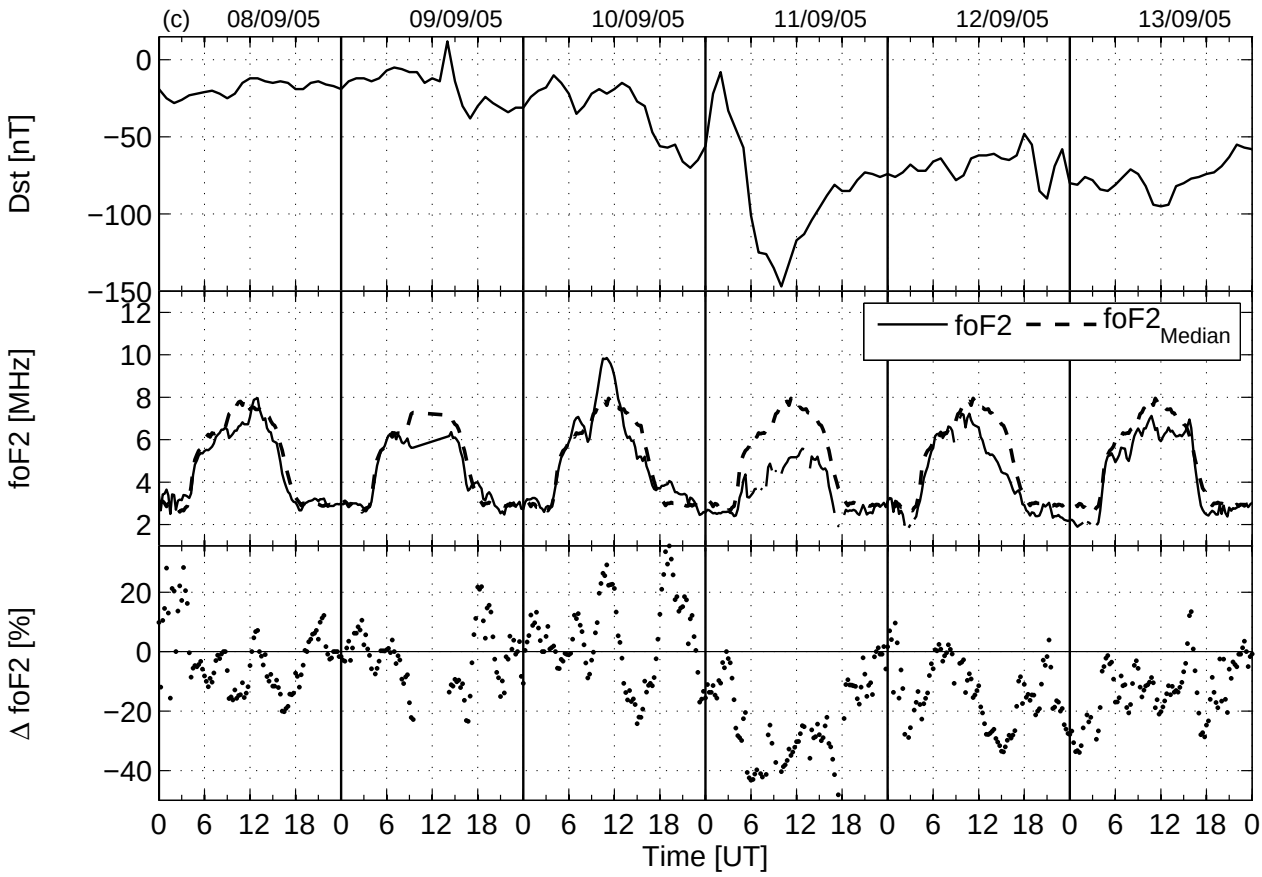

Figure 4.3: An example of PN ionospheric storm effects over Grahamstown (33.3°S, 26.5°E)

Figure 4.4 shows an example of a NP ionospheric storm effect on foF2 for the period 6 to 12 November 2004. The main phase (with a minimum Dst index of −373 nT), which occurred on the 8 November 2004 at 06 : 00 UT, caused a decrease in foF2. It is more evident in the ΔfoF2 which showed a significant decrease of about −53%. During the recovery phase on 9 November 2004 a significant increase of about 30% in ΔfoF2 was observed. Just before the geomagnetic storm of 9 November 2004 fully recovered, another storm occurred with a minimum Dst of −289 nT on 10 November 2004 which caused a depletion in foF2. The deviations in the F2 layer clearly shows the decrease of about −66% in ΔfoF2. The N storm phase on 8, 10 and 11 November 2004 could have been caused by changes in neutral gas composition (Seaton, 1956; Prölss, 1980, 1995, 1997, 2004; Buonsanto, 1999; Zhang et al., 2004; Sahai et al., 2009; Habarulema et al., 2013b). The P storm phase that occurred on 9 November 2004 could be attributed to the large wind circulation and the increase in the O/N_2 ratio. This particular storm period was analysed in detail by Habarulema et al. (2013b) using ionosonde and GPS TEC data which showed a similar response. The depletion in foF2 corresponded to the decrease in the O/N_2 ratio as observed from the Global Ultraviolet Imager (GUVI) maps. Sahai et al. (2009) observed similar responses for the same geomagnetic storm period using VTEC over the Latin American sector ionospheric F region.

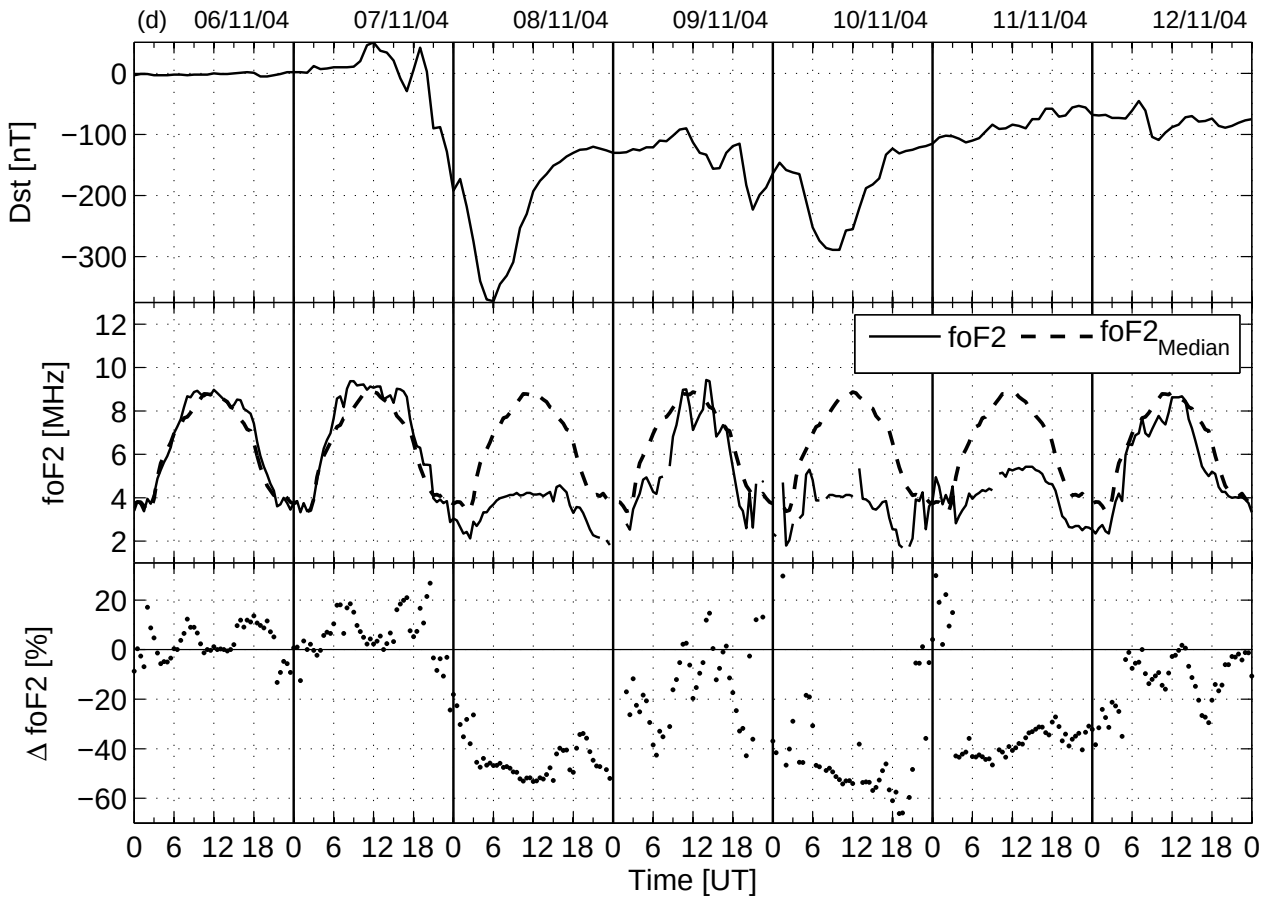

Figure 4.4: An example of NP ionospheric storm effects over Grahamstown (33.3°S, 26.5°E)

Figure 4.5 shows an example of NS ionospheric storm effects for the period 21 to 24 April 2001. The main phase occurred on 22 April 2001 at around 15 : 00 UT and reached a minimum Dst of −103 nT. There was neither a clear increase nor decrease in foF2 compared to the monthly median values, and hence this was classified as a NS ionospheric storm effect. However, Maruyama and Nakamura (2007) studied the same storm period over the Japanese lower mid-latitudes, namely Wakkanai (45.4°N, 141.7°E; 40.5°N magnetic latitude), Kokubunji (35.7°N, 139.5°E; 30.0°N magnetic latitude) and Okinawa (26.3°N, 127.8°E; 20.7°N magnetic latitude) using foF2 and hmF2. They observed P and N ionospheric storms which were attributed to the three cycles of wavy fluctuations in TIDs on the night of 20 March 2001.

In summary, the storm classification was based on percentage deviations of time series foF2 from monthly median values which served as the background ionospheric variability. These percentage deviations were computed according to Equation 4.1 and foF2 variability ranges within ±20% was considered quiet and hence storms which did not show variations outside this range were classified as not significant. For TEC, the quiet time percentage range was determined as ±40% following a similar procedure.

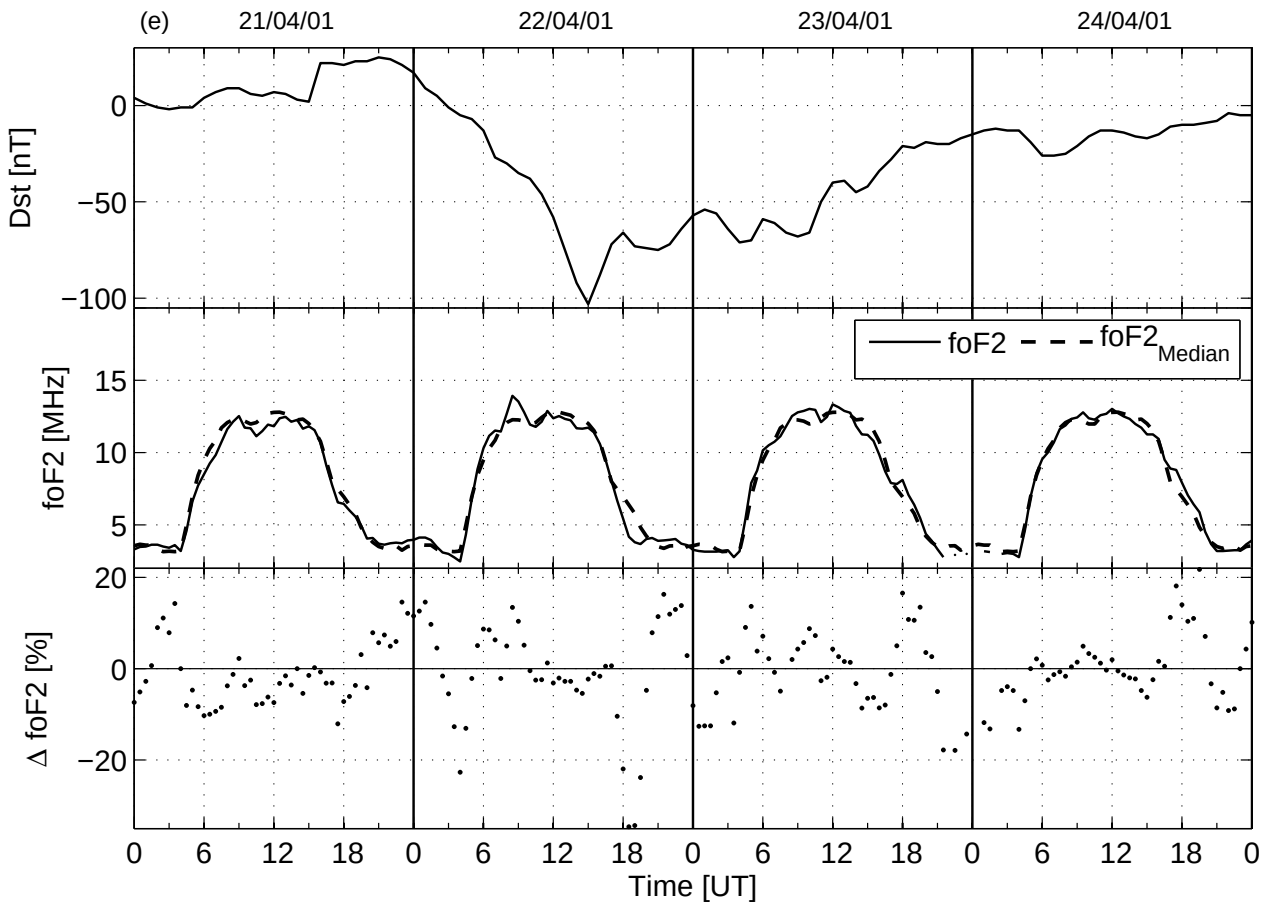

Figure 4.5: An example of NS ionospheric storm effects over Grahamstown (33.3°S, 26.5°E)

4.3.2 Ionospheric storm occurrence in relation to geomagnetic storms and solar activity

The Sun's activity is dominated by flares and CMEs during solar maximum. The predominance of CMEs and IMF conditions cause the development of geomagnetic storms during solar maximum. Large geomagnetic storms are often associated with the CMEs that cause the sudden and large disturbances in the magnetosphere and ionosphere (Tsurutani et al., 2006).

However, during the declining phase away from the solar maximum of the solar cycle, moderate geomagnetic storms under different IMF conditions are generated by the high speed ($\sim$ 750 to 800 km/s) solar wind streams from coronal holes (Tsurutani et al., 2006). If the holes last for more than 27 days, the high speed streams reappear with each solar rotation, and co-rotate with the Sun. If the high speed streams overtake the slower speed ($\sim$ 300 to 400 km/s) stream, their interaction results in both magnetic field and plasma compressions at their interfaces. This happens near the ecliptic plane. For magnetic storms activity, the most important interplanetary features are the intense magnetic field regions called CIRs.

When CIRs strike the Earth's magnetosphere, they may cause magnetic storms, though only weak and moderate in intensity (Tsurutani et al., 1995, 2006).

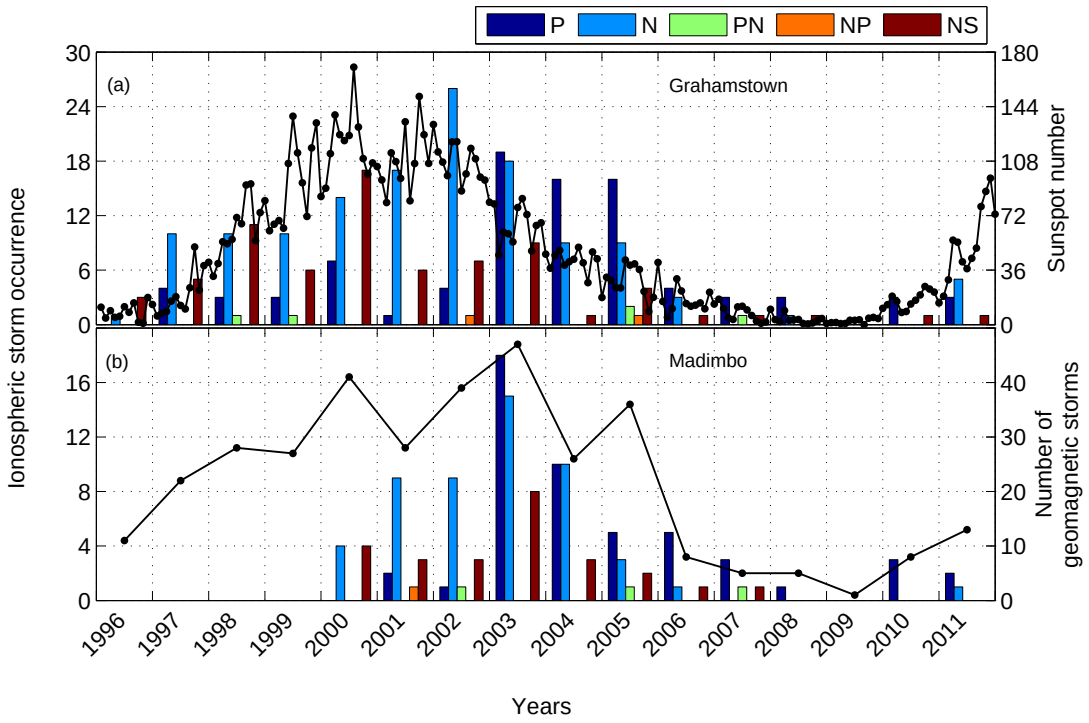

Figure 4.6: Ionospheric storm effect occurrence over Grahamstown (33.3°S, 26.5°E) and Madimbo (22.4°S, 30.9°E) during the period 1996 to 2011. Superimposed are the sunspot number and the annual number of geomagnetic storms for Grahamstown and Madimbo respectively.

Figure 4.6(a) shows the ionospheric storm effects occurrence over Grahamstown during 1996 to 2011. Superimposed on this plot is the sunspot number (monthly sunspot number was downloaded from sidc.oma.be/sunspot-data/). Figure 4.6(b) shows the ionospheric effect occurrence for Madimbo with the annual number of geomagnetic storms superimposed.

Figure 4.6(a) clearly shows that the occurrence of N ionospheric storm effects approximately follow solar activity, with an exception of $1997 - 1998$ when the same number of negative ionospheric storm effects is observed. However Table 4.2 shows that there was some missing data for some geomagnetic storm periods which when considered can possibly change the reported number of N ionospheric storms effects for 1997 and 1998. This is well explained by the mechanisms responsible for N storm effects. Because of the thermal expansion, the background O/N_2 ratio is minimal at solar maximum compared to solar minimum. The already existing small O/N_2 ratio is reduced further, due to storm-induced neutral winds (as a result of joule heating), making conditions favourable for N storm effects to occur more frequently

at solar maximum than at solar minimum (e.g. Prölss, 1995; Vijaya Lekshmi et al., 2011). Available observations over Grahamstown show that the maximum number of N ionospheric storms occurred in 2002. Most P ionospheric storms occurred during the declining phase of the sunspot cycle. This agrees with studies by Buresova et al. (2014), who noted that the long declining phase solar minimum (2007 to 2009) was caused mainly by fast solar wind streams, but not by CMEs and related phenomena. They showed that the effects on the mid-latitude ionosphere caused by a weak-moderate magnetic storm are related to CIR. They found that P effects on foF2 prevailed during the period of low solar activity from 2007 to 2009 and were more significant than negative effects.

Figure 4.6 indicates that NS ionospheric storm effects occur almost all the time, irrespective of the solar activity trend. In general, the occurrence of ionospheric storms decreases with decreasing solar activity. For example, in 2009 only one geomagnetic storm was observed with a minimum Dst ≤ -50 nT. No ionosonde data was available to check the ionospheric storm effect. However, the usage of TEC data revealed a P ionospheric storm effect during the only storm of 2009 as shown in Figure 4.7. During the geomagnetic storm of 22 July 2009, the Dst reached the minimum value of -79 nT at about 09 : 00 UT. The TEC values rapidly increased above the quiet day TEC monthly median values. This is more evident from the TEC deviation increase of $> 100\%$.

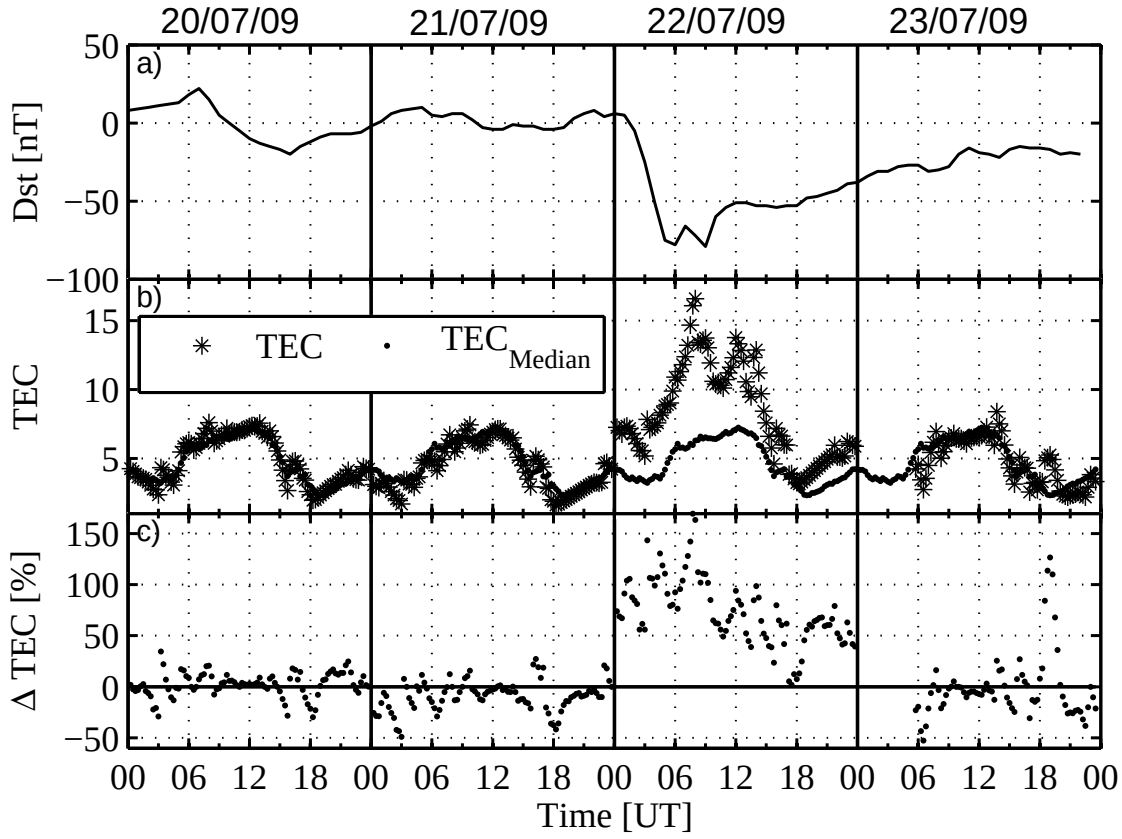

Figure 4.7: P ionospheric storm effect on TEC over Grahamstown (33.3°S, 26.5°E)

Statistically Figure 4.6(b) agrees with Figure 4.6(a), especially for N storm effects. The Madimbo ionosonde station was only installed in August 2000. The peak of the geomagnetic storms occurred in 2003 during the declining phase of the sunspot cycle, when more P ionospheric storms occurred than N ionospheric storms. It is possible that the statistics presented in Figure 4.6(b) would change if all the data were available for the periods during which geomagnetic storms occurred.

The unavailability of the foF2 data for certain periods, led to the investigation of the possibility of using TEC data to derive the ionospheric response to geomagnetic storms. A number of studies have shown that there is a high correlation between TEC and foF2 (e.g. Kouris et al., 2004; Ssessanga et al., 2014) and so it was appropriate to assume that, in the absence of one set of observations, the other set could be used to obtain probable information about ionospheric behaviour. Kouris et al. (2004) found that TEC and $(foF2)^2$ values show a high correlation coefficient greater than 0.80. They also found that the daily variation of TEC is close to that of foF2 during periods of low/medium solar activity. Ssessanga et al. (2014) developed a statistical method (TEC2F2) for estimating foF2 values from GPS VTEC over

the African sector. They found that the TEC2F2 method provides a better correlation with the measured values of foF2, where the high values of R^2 (coefficient of determination) are above 0.8 at both Grahamstown and Hermanus. A study by Balan and Rao (1990) used TEC and N_{max} to analyze the ionospheric response at low and mid-latitudes using geomagnetic storm data for the period 1968 to 1972. Their results showed a systematic dependence of the development of P and N ionospheric storms on the local time of sudden commencement (SC) of geomagnetic storms at both low and mid-latitudes. They found that the storm time deviations in ΔTEC and ΔN_{max} show the same features as the ionospheric response.

Figure 4.8 shows a comparison of TEC and foF2 ionospheric storm effects statistics for Grahamstown during the period 2006 to 2011. For periods where both data sets are available, the derived statistics are the same and both show identical ionospheric storm effects, as shown in Figure 4.8(c-d). The obtained results are important because they successfully show that TEC data complements ionosonde data, even for event analysis.

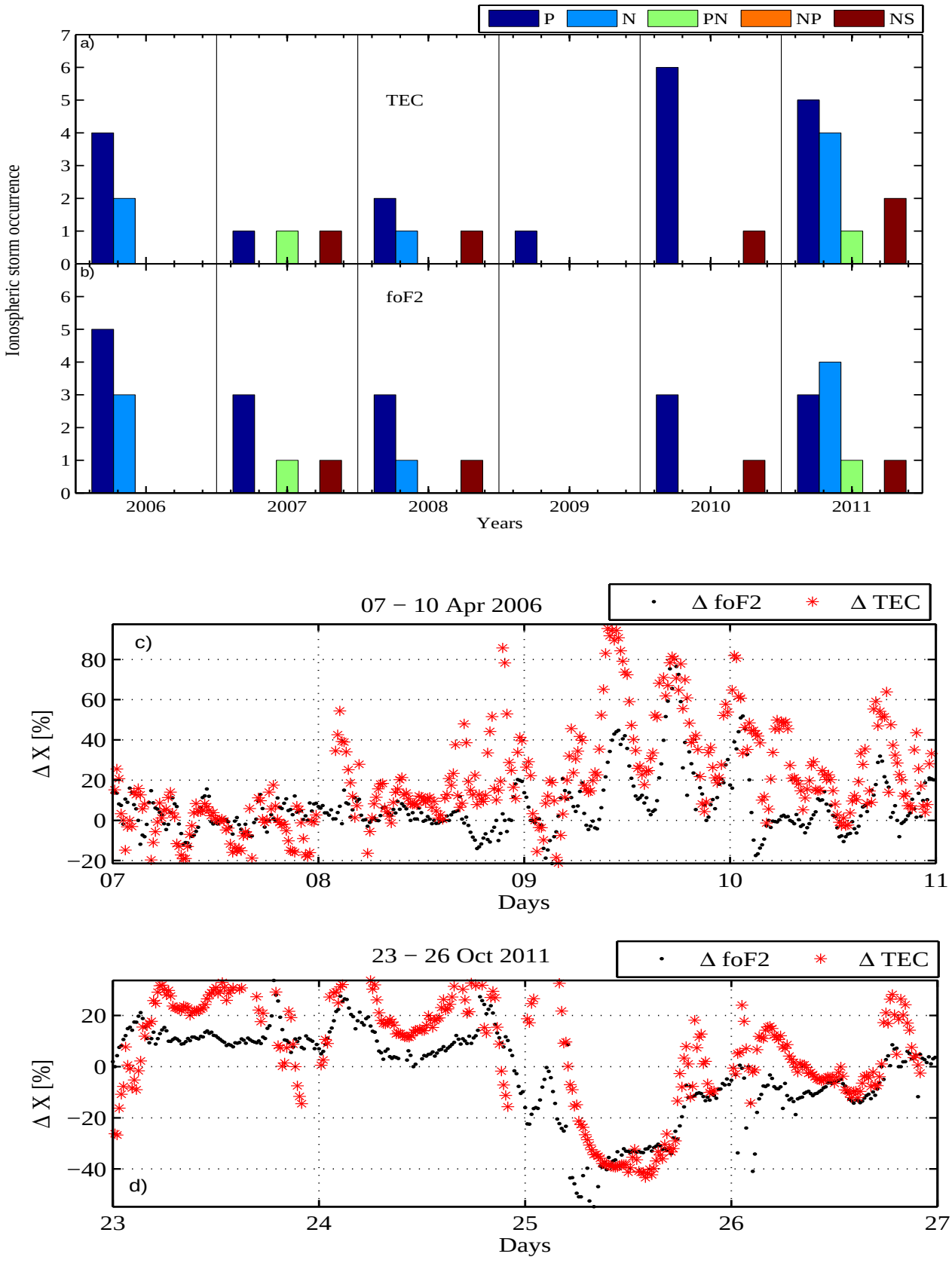

Figure 4.8: Comparison of (a) TEC and (b) foF2 ionospheric storm effects statistics for Grahamstown (33.3°S, 26.5°E) from 2006 to 2011. Examples of deviations showing similar responses for foF2 and TEC during P and N ionospheric storms are also shown.

4.3.3 Ionospheric storm effect analysis according to geomagnetic storm intensity

Occurrence of different classes of ionospheric storm effects, classified according to the intensity of the geomagnetic storm by the Dst classification criteria of Loewe and Prölss (1997) (see Table 4.1), is shown in Figure 4.9.

Figure 4.9(a) shows that most ionospheric storms (78%) occurred during moderate geomagnetic conditions (Dst: -50 to -100 nT). Echer et al. (2013) identified the drivers of the moderate geomagnetic conditions as CIRs, HSSs, ICMEs, sheaths, as well as their combined occurrence. Echer et al. (2013) noted that the annual rate of occurrence of moderate storms had two peaks, one near solar maximum and the other in the descending phase, around 3 years later. In this study most ionospheric response (17.54%) occurred during moderate geomagnetic condition in 2003 (during declining phase of solar cycle 23) and this agrees with the studies by Echer et al. (2013).
A considerable number of NS ionospheric storms occurred during moderate (29%) and strong (9%) geomagnetic condition respectively (as illustrated in Figure 4.9(a) and (b) and Table 4.3). PN ionospheric storms were observed during moderate (2%), strong (3%) and very strong (7%) geomagnetic conditions respectively. While 3% of NP ionospheric storm were observed during strong geomagnetic condition.
During great storms (Figure 4.9(d)) only N ionospheric storm (100%) effects were observed. During large or great storms the foF2 gets depleted and may sometimes drop from its normal value by a factor of 2 (McNamara, 1991), which is due mainly to changes in the neutral composition of the O/N_2 ratio. Most of the intense geomagnetic storms are caused by fast CMEs which induce disturbances in the solar wind. During a period of high solar activity, CMEs occur more frequently. The N ionospheric storms that were observed during great geomagnetic storms (Figure 4.9(d)) occurred during a period of high solar activity. From Figure 4.9 it appears feasible to infer the ionospheric response from the strength of geomagnetic storms as quantified by the Dst index especially for strong to great geomagnetic storms.

Table 4.3: Statistics showing the occurance of ionospheric responses according to geomagneticstorm intensity

Ionospheric response	Moderate [%]	Strong [%]	Very strong [%]	Great [%]
P	33	26	43	0
N	37	58	50	100
PN	2	3	7	0
NP	0	3	0	0
NS	29	9	0	0

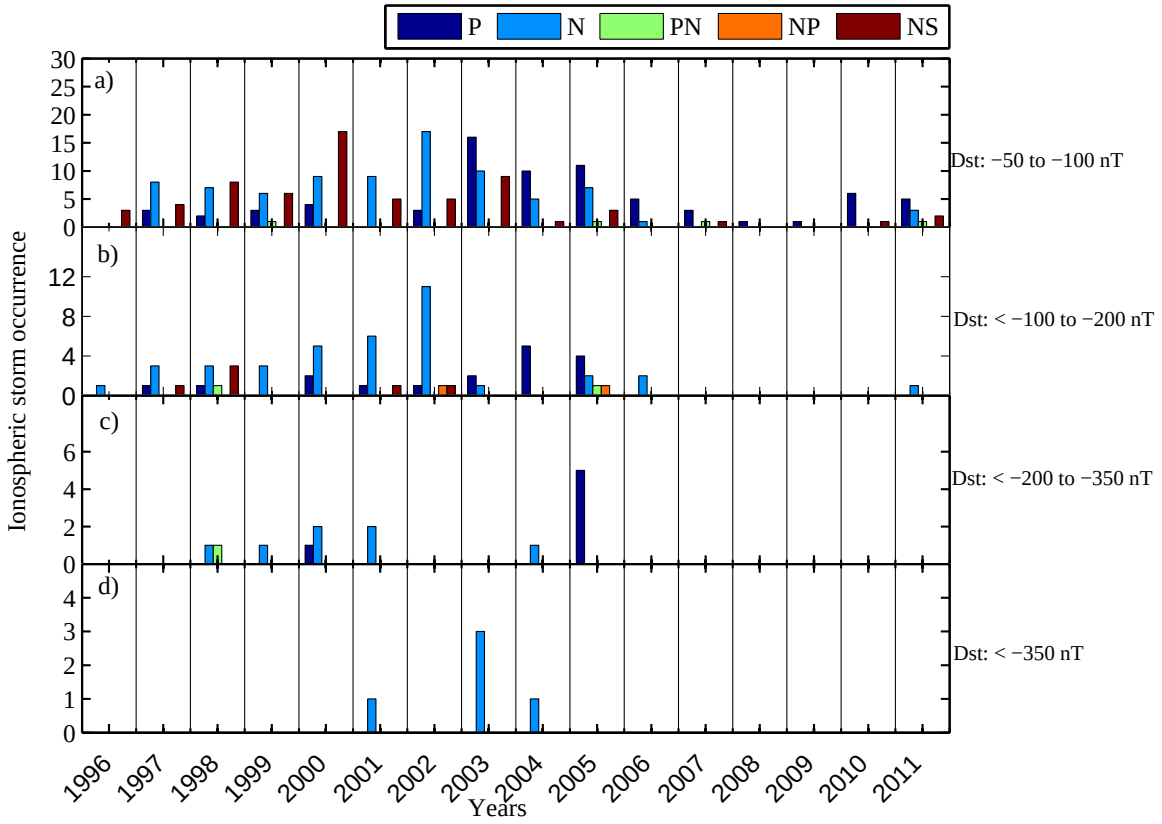

Figure 4.9: Ionospheric storm occurrence over Grahamstown (33.3°S, 26.5°E) according to geomagnetic storm classification ((a) Dst: −50 to −100 nT; (b) Dst: < −100 to −200 nT; (c) Dst: < −200 to −350 nT; and (d) Dst: < −350 nT).

4.3.4 Local time analysis of ionospheric storm effects

Figure 4.10 shows the (a) P, (b) N, (c) PN, (d) NP and (e) NS ionospheric storms occurrence as a function of local time. SAST, or local time, is ahead of UT by 2 hours (i.e. SAST = UT +2 hours). The local time used in this figure is the time corresponding to the minimum Dst (Peak of the main phase) for each storm.

Figure 4.10(a) shows that most P ionospheric storms occurred between 06:00 and 15:00 LT with the maximum occurring at 10:00 LT. Prölss (1995) previously reported that most P ionospheric storms over mid-latitudes are generally associated with geomagnetic activity beginning in the local daytime sector. This is because P storm effects contribute to the daytime ionisation production on top of the minimal chemical loss that exists during local daytime (e.g. Kelley et al., 2004).

Figure 4.10(b) shows that there appears to be no dominant local time for the occurrence

of N ionospheric effects, apart from the isolated incidence at 08:00 and 23:00 LT. Gao et al. (2008) also reported the two maxima in N ionospheric storm occurrence in early morning and pre-midnight local time. These observations agree with the studies by Gao et al. (2008) and Vijaya Lekshmi et al. (2011). The two N ionospheric storm effect maxima may be due to the zonal transport of composition changes by advection. During the morning and midnight sectors the strong winds carry air from disturbed composition out of the heating region towards the mid-latitudes. This region is swamped with air of enhanced molecular content and the ionosonde station located under this region will observe a N ionospheric storm effect. The nighttime N effects are due to low ionisation density at night and the equatorward winds may slow down the ionisation loss processes. During very strong storms the heating zone and the associated composition perturbations may expand into what are normally considered mid-latitudes even in the day sector (Prölss, 1993*b*).

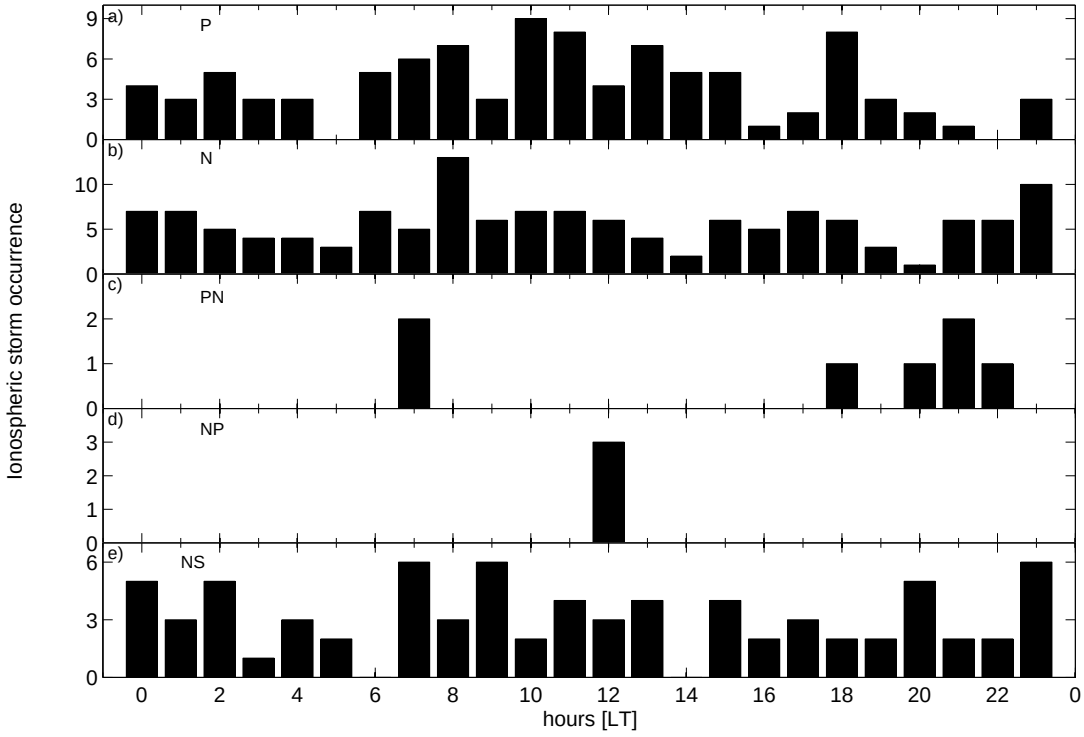

Figure 4.10: The relationship between ionospheric storms ((a) P; (b) N; (c) PN; (d) NP; and (e) NS) and local time over Grahamstown (33.3°S, 26.5°E).

Figure 4.11 illustrates the dependence of ionospheric storms on local time during season (summer, winter, autumn and spring). The seasonal categorisation was done according to Table 4.4.

During the summer, few P ionospheric storm effects occurred, the maximum number of storms

Table 4.4: Seasonal calender obtained from *South African Weather Service* (2013)

Seasons	**Month**
Autumn	1 March to 31 May
Winter	1 June to 31 August
Spring	1 September to 30 November
Summer	1 December to 28/29 February

(3) occurring at 18:00 LT and some occurred at 10:00 to 12:00 LT. However, N ionospheric storm effects occurred more often during the summer with a maximum number of ionospheric storm effects occurring at 23:00 LT. There is no dominant local time for the occurrence of N ionospheric storms in summer. This is because the quiet time storm-induced thermospheric circulation makes the ratio of background oxygen to molecular nitrogen (O/N_2) smaller during the summer, and causes the electron density of the F2 layer to decrease (Vijaya Lekshmi et al., 2011; Danilov, 2013). No double disturbance storms were observed during the summer. Only two NS ionospheric storms occurred at 23:00 LT during the summer.

During the winter, most P ionospheric storm effects occurred during the day and a few occurred at night. Only five N ionospheric storm effects occurred and there is no local time when these storms dominate. One double disturbance storm occurred at 21:00 LT.

During the autumn, most P ionospheric storms occurred during the day with a maximum occurring at 10:00 LT. N ionospheric storms occurred during both the night and morning local time, while PN only occurred at 07:00 LT.

During the spring, most ionospheric storm effects that occurred were N with a maximum number of ionospheric storm effects occurring at 08:00 LT. Few P ionospheric storms were observed with a maximum occurring at 07:00 LT. Only four PN ionospheric storms occurred at night, namely at 18:00 and 20:00 to 22:00 LT. Only two NP ionospheric storm effects occurred at 12:00 LT. It appears that NS storms effects may be observed at any time.

These observations agree with the observations by Rodger et al. (1989), who showed that the ionospheric response reveals both local time and seasonal variations during geomagnetic storms. They demonstrated that over a mid-latitude station, the local time signature in the ratio of quiet to disturbed maximum electron concentration of the F2 layer (NmF2) is consistent and exists throughout the year.

Prölss (1993*b*) suggested that the N storm effects are due to regions in which the neutral gas composition is changed and the O/N_2 ratio is increased. This region is called a composition bulge, because it represents a region of increased mean mass. It is produced through heating and upwelling of air by magnetospheric energy inputs at auroral latitudes. The bulge may be moved to the mid-latitudes by the nightside equatorward winds and brought onto the dayside as the Earth rotates. Rodger et al. (1989) attributed the local time diurnal variation of NmF2 effects to an oscillation in latitude of the composition bulge in response to the diurnally varying winds.

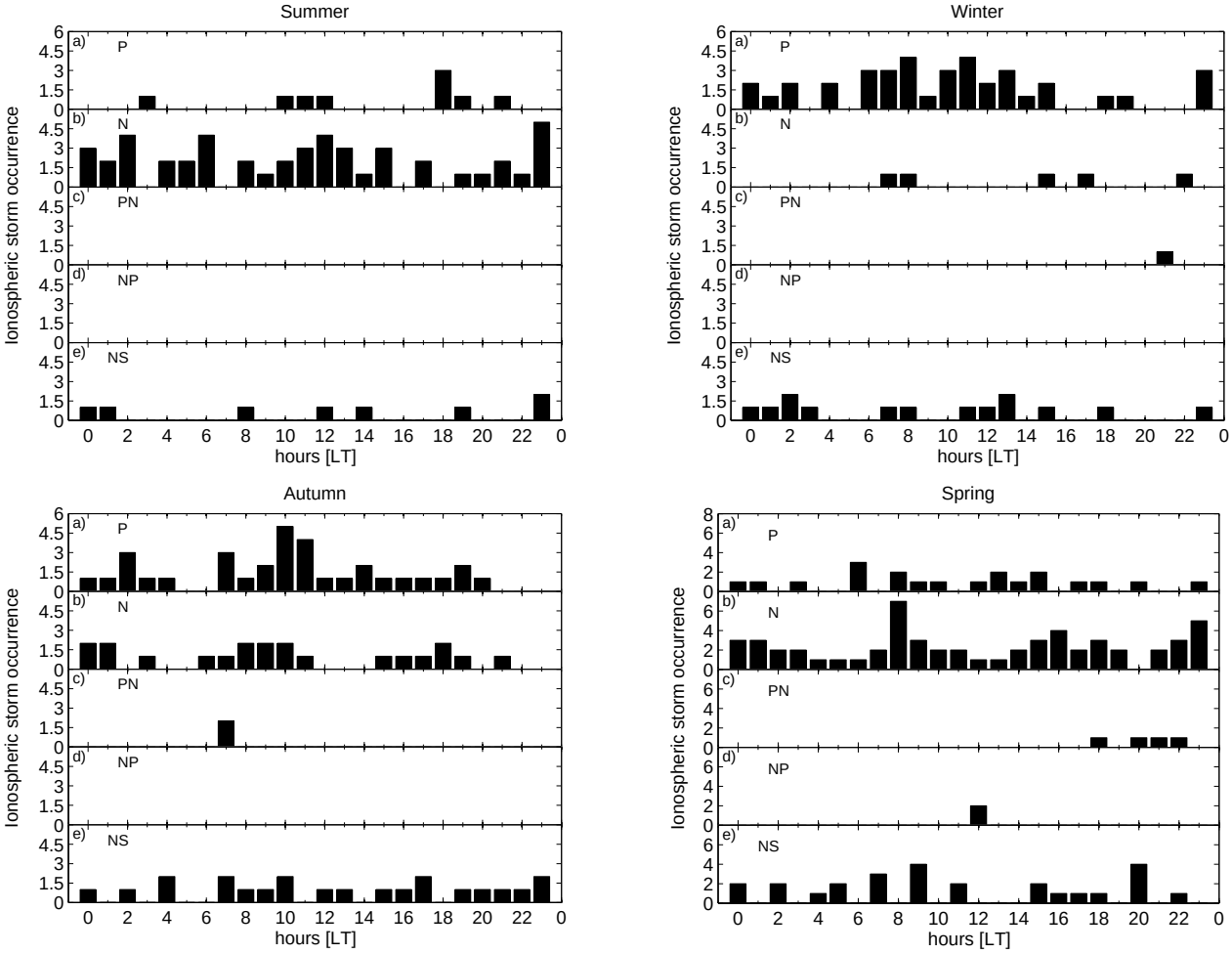

Figure 4.11: The dependence of ionospheric storms on local time during summer, winter, autumn and spring over Grahamstown (33.3°S, 26.5°E).

4.3.5 Seasonal dependence of ionospheric storm effects on solar activity

The available foF2 data (1996 to 2011) for all storm periods identified over Grahamstown (33.3°S, 26.5°E) was categorised by season as described in Table 4.4.

The seasonal variation in ionospheric storm effects are believed to arise from the interaction between the seasonal and storm-induced winds. Both these winds support each other in summer, but in winter they are out of phase (Prölss, 1995). The seasonal effect is also believed to be caused by a bulge which prevails during summer due to wind circulation (Fuller-Rowell et al., 1997).

Figure 4.12 shows the seasonal dependence of ionospheric storm effects for (a) Summer, (b) Autumn, (c) Winter and (d) Spring over Grahamstown (33.3°S, 26.5°E) for the period 1996 to 2011. Most ionospheric storms occurred during equinox (spring and autumn). Most P and N ionospheric storms occurred during winter and summer respectively. This agrees with the studies by Prölss (1980, 1995); Fuller-Rowell et al. (1996, 1997); Gao et al. (2008); Vijaya Lekshmi et al. (2011). The occurrence of P ionospheric storms during the winter months may be due to the limited extent of the composition disturbance zone (Prölss, 1995).

During the equinoxes, N ionospheric storm effects occurred most frequently in spring, while in autumn P and N ionospheric storms have a relatively similar distribution. Very few cases of N ionospheric storms are seen during winter. The occurrence of N ionospheric storms summer is related to the thermal expansion mechanism which causes a smaller O/N_2 ratio in summer than in winter, with additional reduction being accelerated by storm-induced neutral winds. During the summer there were few NS storms and a complete absence of double disturbance ionospheric storm effects. Generally, the NS storm effects do not have a seasonal pattern, but rather follow the distribution of the geomagnetic storms (Vijaya Lekshmi et al., 2011). The seasonal results of this study agree with previous studies (e.g. Prölss, 1995; Vijaya Lekshmi et al., 2011).

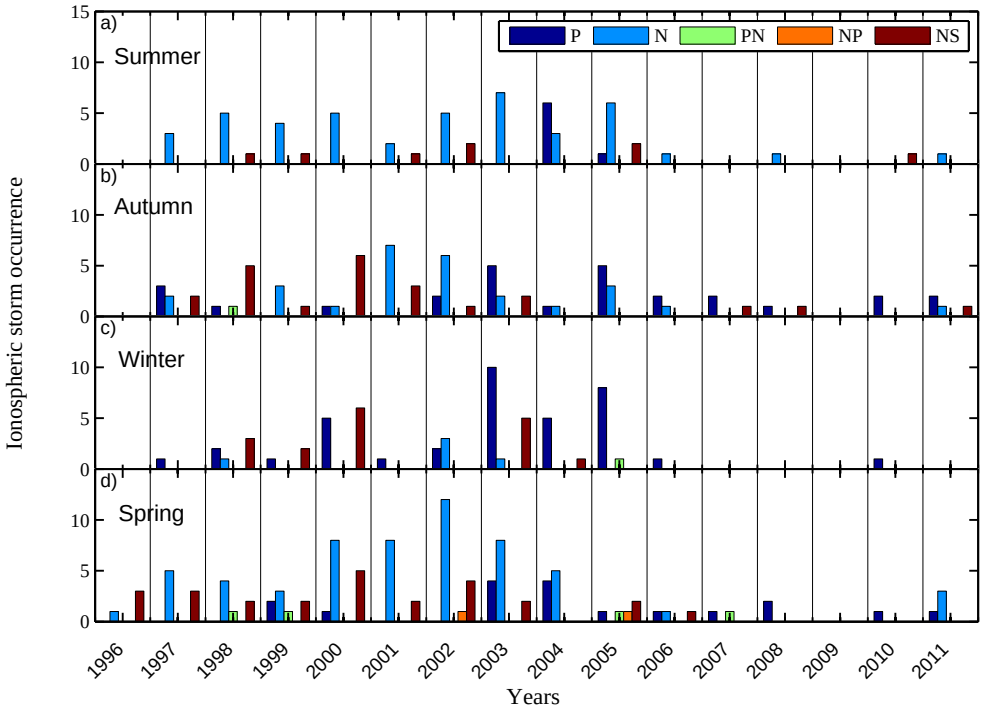

Figure 4.12: Seasonal dependence of ionospheric storm occurrence over Grahamstown (33.3°S, 26.5°E).

4.4 Conclusion

A statistical analysis of ionospheric storm effects over Grahamstown (33.3°S, 26.5°E) and Madimbo (22.4°S, 30.9°E), South Africa was done using a storm criterion of Dst ≤ -50 nT. The method used for identifying the ionospheric storm effects using ionosonde data is described in this chapter. The statistics of the ionospheric storm effects observed during geomagnetic storms are presented. Different classes of ionospheric storms were classified as P, N, PN, NP and NS ionospheric storms. The behaviour of N ionospheric storms follows solar activity patterns. The usage of TEC data derived from GPS observations to identify the types of ionospheric storm effects in the absence of ionosonde data was investigated, and proved to be successful. TEC observations were limited to near-vertical observations, using only satellites with an elevation angle greater than 60 degrees. For the periods when foF2 and TEC datasets are available, identical ionospheric responses were observed and it was statistically shown that TEC can be used when foF2 data is unavailable and vice versa. Most N and P ionospheric storms occurred in 2002 and 2003 respectively. The results of this study generally agree with previous findings for mid-latitude regions (Gao et al., 2008; Vijaya Lekshmi et al., 2011), but have also given some new insights. For example, it was

shown that only N ionospheric storms occurred during great storms (Dst < -350 nT). Most P and NS ionospheric storms occurred during moderate storms (Dst: -50 to -100 nT). For storms with a Dst strength of Dst < -100 nT, these results show that it is possible to predict the behaviour of the ionospheric foF2 or electron density, as long as the strength of the storm is predictable. P ionospheric storms frequently occurred during the morning. N and P ionospheric storms occurred more often during summer and winter respectively.

Chapter 5

Summary and future work

5.1 Introduction

Perturbations within the ionosphere due to an increase in the dissipation of solar wind energy remains one of the challenging subjects for ionospheric physics. These disturbances have a great influence on the global structure of the ionosphere. Ionospheric perturbations are of practical interest because they have the potential to degrade trans-ionospheric and HF radio communications, and are therefore of importance to space weather applications. During geomagnetic storms all ionospheric parameters are affected (Prölss, 1995). The foF2 and GPS TEC are the most commonly used parameters for studying ionospheric storm responses during geomagnetic storms (e.g. Balan and Rao, 1990; Danilov, 2001; Gao et al., 2008)

Gao et al. (2008) used foF2 observed from 4 ionosonde stations in the East Asian sector over low and mid-latitudes to statistically analyse ionospheric storm effects observed during geomagnetic storms from 1957 to 2006. Vijaya Lekshmi et al. (2011) used the peak electron density to statistically analyse the effects of geomagnetic storms at Kukubunji (35.7°N, 139.5°E; 26.8°N magnetic latitude) and Boulder (40.0°N, 254.7°E; 47.4°N magnetic latitude), from 1985 to 2005, i.e. over 2 solar cycles. These studies observed single and double disturbances as well as no significant effects during storm conditions.

This chapter summarises the results discussed in previous chapters, and briefly discusses the limitations encountered. The objective of the study was to carry out a statistical analysis of the ionospheric response during geomagnetic storms over the mid-latitude stations Grahamstown (33.3°S, 26.5°E) and Madimbo (22.4°S, 30.9°E), South Africa. This was achieved by studying the variability of foF2 and TEC during geomagnetic storm conditions during the period 1996 to 2011. The storm criterion of Dst ≤ -50 nT was used to identify the geomagnetic storm periods. A total of 346 geomagnetic storms were recorded during the period 1996 to 2011. Due to the availability of long-term historic and reliable data, the conclusions of this work were based mainly on Grahamstown data. Of the 346 recorded geomagnetic storms, the ionospheric storm effects of 308 (89.02%) were observed at the Grahamstown

ionosonde station between 1996 to 2011.

5.2 Summary

In this study foF2 and GPS TEC data was used to analyse the ionospheric responses during geomagnetic storms over the Southern Africa mid-latitudes. The classification of ionospheric storm effects by Vijaya Lekshmi et al. (2011) was used in this study.

Five classes of ionospheric storm effects were identified, namely positive (P) (29%), negative (N) (44%), positive followed by negative (PN) (2%), negative followed by positive (NP) (1%), and not significant (NS) (24%) ionospheric storm effects observed over the period ranging from 1996 to 2011. The percentage deviation of TEC or foF2 from their respective monthly median values were used to identify the type of ionospheric storm effect during geomagnetic storms.

The statistics of ionospheric storm effects over Grahamstown were analysed with respect to the solar cycle, storm intensity, local time, and seasonal dependence.

It was found that N ionospheric storm effects follow the trend of the solar cycle with the most responses occurring at solar maximum. This agrees with the study by Vijaya Lekshmi et al. (2011). The quiet time O/N_2 ratio at all pressure levels is smaller at solar maximum than at solar minimum due to thermal expansion. In such a background thermosphere, the chemical effects of the storm-time neutral winds can easily make the O/N_2 ratio much smaller at solar maximum than at solar minimum. Hence, N ionospheric storms can easily occur during solar maximum than solar minimum (Vijaya Lekshmi et al., 2011). It was observed that P ionospheric storms do not follow the solar cycle trend. Most P ionospheric storm effects occurred during the declining phase of the solar cycle. This agrees with the studies by Vijaya Lekshmi et al. (2011) and Buresova et al. (2014). It was found that NS ionospheric storm effects also do not follow the solar cycle trend, but rather follow the distribution of geomagnetic storms.

The storm intensity analysis was based on the Dst classification criterion by Loewe and Prölss (1997). It was found that during moderate geomagnetic conditions most ionospheric storm effects occurred. Most N ionospheric storm effects occurred during strong (Dst $<$ -100 to -200 nT) and very strong (Dst <-200 to -350 nT) geomagnetic storms. During the solar minimum in 2009, only P ionospheric storms occurred. This agrees with studies by Buresova et al. (2014) which show that most P storms occurred during the solar minimum of solar cycle 23/24 and were due to CIRs. An important finding is that during great geo-

magnetic conditions (Dst ≤ -350 nT) only N ionospheric storm effects occurred.

The statistics revealed that P ionospheric storms frequently occurred during the morning to noon local time (i.e. between 06:00 - 15:00 LT with a maximum at 10:00 LT) and N ionospheric storms mostly occurred at night and in the morning local time (i.e. 08:00 and 23:00 LT). These results agree with studies by Prölss (1995), Gao et al. (2008) and Vijaya Lekshmi et al. (2011).

It was found that most N ionospheric storm effects (63.24%) occurred during the summer and most P ionospheric storm effects (53.62%) occurred during the winter. These results agree with the literature (Prölss, 1995; Buonsanto, 1999) and the observations (Gao et al., 2008; Vijaya Lekshmi et al., 2011). The seasonal variations are believed to arise from the interaction between the seasonal and storm-induced winds. These winds support each other during the summer, but during the winter they are out of phase (Prölss, 1995).

An analysis of GPS TEC data shows that it may be used to compliment ionosonde data for event analysis. This was done by comparing the ionospheric storm effects obtained from foF2 and TEC over Grahamstown during the period 2006 to 2011. For the periods where both datasets were available the derived statistics were the same and both show identical ionospheric effects.

5.3 Limitations

The conclusions of this study are based on foF2 measurements from the Grahamstown (33.3°S, 26.5°E) station. Here only 89.02% of geomagnetic storms were considered to analyse the variability of foF2. Of the 346 geomagnetic storms that occurred between 2000 to 2011, the ionosonde data for only 37.86% was available at Madimbo (22.4°S, 30.9°E) station, which only started operation in mid-August 2000. Also out of 260 geomagnetic storms that occurred between 2000 to 2011 only 50.38% of foF2 data over Madimbo was available to check the ionospheric responses of foF2 during geomagnetic storms. Due to this data paucity it was not possible to do a complete statistical analysis of the ionosperic storm responses over this station.

5.4 Future work

This study was restricted to ionospheric responses over South African mid-latitudes. It is important if be extended to the low and equatorial latitudes of Africa. Goals for future studies may include:

- Investigate the causes of variations of ionospheric storms with geomagnetic latitude (low latitude, mid-latitude and equatorial latitude).
- Explain or establish the physical mechanisms that drive ionospheric responses over the geomagnetic latitude regions within the African sector, making use of long-term historic data.
- to provide a full understanding of ionospheric storm effects with respect to solar cycle variations.

References

Adewale, A. O., Oyeyemi, E. O., Adeloye, A. B., Ngwira, C. M. and Athieno, R. (2011), 'Responses of equatorial F region to different geomagnetic storms observed by GPS in the African sector', *Journal of Geophysical Research* **116**(A12), A12319.

Amabayo, E. B., McKinnell, L. A. and Cilliers, P. J. (2012), 'Ionospheric response over South Africa to the geomagnetic storm of 11–13 April 2001', *Journal of Atmospheric and Solar-Terrestrial Physics* **84–85**, 62–74.

Balan, N. and Rao, P. (1990), 'Dependence of ionospheric response on the local time of sudden commencement and the intensity of geomagnetic storms', *Journal of Atmospheric and Terrestrial Physics* **52**(4), 269–275.

Balan, N., Shiokawa, K., Otsuka, Y., Kikuchi, T., Vijaya Lekshmi, D., Kawamura, S., Yamamoto, M. and Bailey, G. J. (2010), 'A physical mechanism of positive ionospheric storms at low latitudes and midlatitudes', *Journal of Geophysical Research* **115**(A2), A02304.

Buonsanto, M. (1999), 'Ionospheric storms — a review', *Space Science Reviews* **88**(3-4), 563–601.

Buresova, D., Lastovicka, J., Hejda, P. and Bochnicek, J. (2014), 'Ionospheric disturbances under low solar activity conditions', *Advances in Space Research* **54**(2), 185–196.

Cane, H. V. (1997), The current status in our understanding of energetic particles, coronal mass ejections, and flares, *in* N. Crooker, J. A. Joselyn and J. Feynman, eds, '*Coronal mass ejections*', American Geophysical Union, Washington D.C., pp. 205–215.

Chun, F. K., Knipp, D. J., McHarg, M. G., Lacey, J. R., Lu, G. and Emery, B. A. (2002), 'Joule heating patterns as a function of polar cap index', *Journal of Geophysical Research* **107**(A7), SIA 8–1–SIA 8–9.

Danilov, A. (2001), 'F2-region response to geomagnetic disturbances', *Journal of Atmospheric and Solar-Terrestrial Physics* **63**(5), 441–449.

Danilov, A. D. (2013), 'Ionospheric F-region response to geomagnetic disturbances', *Advances in Space Research* **52**, 343–366.

Davies, K. (1990), *Ionospheric radio*, Peter Peregrinus, London.

Davies, K. and Hartmann, G. K. (1997), 'Studying the ionosphere with the Global Positioning System', *Radio Science* **32**(4), 1695–1703.

Echer, E., Tsurutani, B. T. and Gonzalez, W. D. (2013), 'Interplanetary origins of moderate (100 nT $<$ Dst $\leq$ 50 nT) geomagnetic storms during solar cycle 23 (1996–2008)', *Journal of Geophysical Research: Space Physics* **118**(1), 385–392.

ESA (2015), 'Radio 'sreams' form the Sun warn of radiation storms', `http://www.esa.int/Our\_Activities/Space\_Science/Radio\_screams\_from\_the\_Sun\_warn\_of\_radiation\_storms/\%28print\%29`. (Accessed 2014-02-26).

Farrell, J. and Barth, M. (1998), *The global positioning system and inertial navigation*, McGraw-Hill, New York.

Fuller-Rowell, T. J., Codrescu, M. V., Rishbeth, H., Moffett, R. J. and Quegan, S. (1996), 'On the seasonal response of the thermosphere and ionosphere to geomagnetic storms', *Journal of Geophysical Research* **101**(A2), 2343–2353.

Fuller-Rowell, T. J., Codrescu, M. V., Roble, R. G. and Richmond, A. D. (1997), How does the thermosphere and ionosphere react to a geomagnetic storm?, *in* B. Tsurutani, W. Gonzalez, Y. Kamide and J. Arballo, eds, '*Magnetic Storms*', American Geophysical Union, Washington D.C., pp. 203–225.

Gao, Q., Liu, L.-B., Zhao, B.-Q., Wan, W.-X., Zhang, M.-L. and Ming, B.-Q. (2008), 'Statistical study of the storm effects in middle latitude ionosphere in the East Asian sector', *Chinese Journal of Geophysics* **51**(3), 435–443.

Gonzalez-Esparza, A. and Aguilar-Rodriguez, E. (2009), 'Speed evolution of fast CME/shocks with SOHO/LASCO, WIND/WAVES, IPS and in-situ WIND data: analysis of kilometric type-II emissions', *Annales Geophysicae* **27**(10), 3957–3966.

Gopalswamy, N. (2006), 'Consequences of coronal mass ejections in the heliosphere', *Sun and Geospace* **1**(2), 5–12.

Gps.gov (2014), 'Official U.S. Government information about the Global Positioning System (GPS) and related topics', `http:www.gps.gov/systems/gps/control/\#personnel`. (Accessed 2014-08-20).

Habarulema, J. B., Katamzi, Z. T. and McKinnell, L. A. (2013a), 'Estimating the propagation characteristics of large-scale travelling ionospheric disturbances using ground-based and satellite data', *Journal of Geophysical Research* **118**(A12), 7768–7782.

Habarulema, J. B., McKinnell, L. A., Burešová, D., Zhang, Y., Seemala, G., Ngwira, C. M., Chum, J. and Opperman, B. (2013b), 'A comparative study of TEC response for the South African equatorial and mid-latitudes during storm conditions', *Journal of Atmospheric and Solar-Terrestrial Physics* **102**, 105–114.

Habarulema, J. B., McKinnell, L. A. and Opperman, B. D. L. (2010), 'TEC measurements and modelling over Southern Africa during magnetic storms; a comparative analysis', *Journal of Atmospheric and Solar-Terrestrial Physics* **72**(5-6), 509–520.

Hofmann-Wellenhof, B., Lichtenegger, H. and Collins, J. (1997), *GPS theory and practice*, 4th edn, Springer Verlag, Vienna.

Hunsucker, R. D. and Hargreaves, J. K. (2003), *The high-latitude ionosphere and its effects on radio propagation*, Cambridge University Press, Cambridge.

Jung, M. and Prölss, G. (1978), 'Numerical simulation of negative ionospheric storms using observed neutral composition data', *Journal of Atmospheric and Terrestrial Physics* **40**, 1347–1350.

Kamide, Y. and Chian, C. A. (2007), An overview of the solar-terrestrial environment , *in* Y. Kamide and A.-L. Chian, eds, '*Handbook of the solar-terrestrial environment*', Springer Verlag, Berlin, pp. 2–22.

Kamide, Y. and Malsev, Y. P. (2007), Geomagnetic storms, *in* Y. Kamide and A. C.-L. Chian, eds, '*Handbook of the solar - terrestrial environment*', Springer Verlag, Berlin, pp. 355–374.

Kaplan, E. D. and Hegarty, C. J. (2006), *Understanding GPS principles and applications*, 2nd edn, Artech House, Boston.

Katamzi, Z., Smith, N., Mitchell, C., Spalla, P. and Materassi, M. (2012), 'Statistical analysis of travelling ionospheric disturbances using TEC observations from geostationary satellites', *Journal of Atmospheric and Solar-Terrestrial Physics* **74**, 64–80.

Katamzi, Z. T. and Habarulema, J. B. (2014), 'Traveling ionospheric disturbances observed at South African midlatitudes during the 29–31 October 2003 geomagnetically disturbed period', *Advances in Space Research* **53**(1), 48–62.

Kelley, M. C., Vlasov, M. N., Foster, J. C. and Coster, A. J. (2004), 'A quantitative explanation for the phenomenon known as storm-enhanced density', *Geophysical Research Letters* **31**(19), L19809.

Kirby, S. S., Gilliland, T. R., Smith, N. and Reymer, S. E. (1936), 'The ionosphere, solar eclipse and magnetic storm', *Physical Review* **50**, 258–259.

Koskinen, E. J. H. (2011), *Physics of space storms: from the solar surface to the Earth*, Springer, Heidelberg.

Kouris, S. S., Xenos, T. D., Polimeris, K. V. and Stergiou, D. (2004), 'TEC and foF2 variations: preliminary results', *Annals of Geophysics* **47**(4), 1325–1332.

Kutner, M. L. (2003), *Astronomy: a physical perpective*, Cambridge University Press, Cambridge.

Loewe, C. A. and Prölss, G. W. (1997), 'Classification and mean behavior of magnetic storms', *Journal of Geophysical Research* **102**(A7), 14209 – 14213.

Lu, G., Goncharenko, L., Coster, A., Richmond, A., Roble, R., Aponte, N. and Paxton, L. J. (2008), A data-model comparative study of ionospheric positive storm phase in the midlatitude F region, *in* P. Kintner, A. Coster, T. Fuller-Rowell, A. Mannucci, M. Mendillo and R. Heelis, eds, '*Midlatitude ionospheric dynamics and disturbances*', 181, pp. 63–75.

Maruyama, T. and Nakamura, M. (2007), 'Conditions for intense ionospheric storms expanding to lower midlatitudes', *Journal of Geophysical Research* **112**(A5), A05310.

Mayer, H. G., Harris, I. and Spencer, N. W. (1978), 'Some properties of upper atmosphere dynamics', *Reviews of Geophysics* **16**(4), 539–565.

Mayr, H. G. and Volland, H. (1972), 'Magnetic storm effects in the neutral composition', *Planetary and Space Science* **20**(3), 379–393.

McNamara, L. F. (1991), *The ionosphere: communications, surveillance and direction finding*, Kriger Publishing, Malabar FL.

Miesch, M. (2005), 'Large scale dynamics of the convection zone and tachocline', `http://www.livingreviews.org/lrsp-2005-1`. (Accessed 2014-05-20).

Miller, K. L., Richards, P. G. and Torr, D. G. (1989), The derivation of meridional neutral winds in thermosphere from F2-layer height, *in* C. Liu, ed., '*World ionosphere / thermosphere study*', chapter 16, pp. 439–471.

Misra, P. and Enge, P. (2006), *Global positioning system: signals, measurements, and performance*, 2nd edn, Ganga-Jamurna Press, Lincoln VA.

Moldwin, M. (2008), *An introduction to space weather*, Cambridge University Press, Cambridge.

Ngwira, C. M. (2011), An analysis of ionospheric response to geomagnetic disturbances over South Africa and Antarctica, PhD thesis, Rhodes University, Grahamstown, South Africa.

Ngwira, C. M., McKinnell, L. A., Cilliers, P. J. and Yizengaw, E. (2012a), 'An investigation of ionospheric disturbances over South Africa during the magnetic storm on 15 May 2005', *Advances in Space Research* **49**, 327–335.

Ngwira, C., McKinnell, L., Cilliers, P. J. and Coster, A. (2012b), 'Ionospheric observations during the geomagnetic storm events on 24-27 July 2004: long-duration positive storm effects ', *Journal of Geophysical Research* **117**(A9), A00L02.

Ondoh, T. and Marubashi, K., eds (2000), *Science of space environment* , Ohmsha, Tokyo.

Opperman, B. D. L. (2007), Reconstructing ionospheric TEC over South Africa using signals from a regional GPS network, PhD thesis, Rhodes University, Grahamstown.

Otto, A. (2005), The magnetosphere, *in* K. Scherer, H. Fichtner, B. Heber and U. Mall, eds, '*Space weather: the physics behind a slogan*', Springer Verlag, Berlin, pp. 133–187.

Parkinson, W. B., Spilker, J. J., Enge, p. and Axelrad, P. (1996), *Global positioning system: theory and applications*, Vol. 1, 5 edn, American Institute of Aeronautics and Astronautics, Michigan.

Prölss, G. (1997), Magnetic storm associated perturbations of the upper atmosphere, *in* B. Tsurutani, W. Gonzalez, Y. Kamide and J. Arballo, eds, '*Magnetic Storms*', American Geophysical Union, Washington D.C., pp. 227–241.

Prölss, G. (2008), Ionospheric storms at mid-latitude: a short review, *in* P. Kintner, A. Coster, T. Fuller-Rowell, A. Mannucci, M. Mendillo and R. Heelis, eds, '*Midlatitude ionospheric dynamics and disturbances*', American Geophysical Union, Washington, DC, pp. 9 –24.

Prölss, G. and Jung, M. (1978), 'Travelling atmospheric disturbances as a possible explanation for daytime positive storm effects of moderate duration at middle latitudes', *Journal of Atmospheric and Terrestrial Physics* **40**(12), 1351–1354.

Prölss, G. W. (1980), 'Magnetic storm associated perturbations of the upper atmosphere: recent results obtained by satellite-borne gas analyzers', *Reviews of Geophysics* **18**(1), 183–202.

Prölss, G. W. (1993*a*), 'Common origin of positive ionospheric storms at middle latitudes and the geomagnetic activity effect at low latitudes', *Journal of Geophysical Research* **98**(A4), 5981–5991.

Prölss, G. W. (1993*b*), 'On explaining the local time variation of the ionospheric storm effects', *Annales Geophysicae* **11**, 1–9.

Prölss, G. W. (1995), Ionospheric F-region storms, *in* H. Volland, ed., '*Handbook of the atmospheric electrodynamics*', Vol. 2, CRC Press, Bonn, chapter 8, pp. 195–248.

Prölss, G. W. (2004), *Physics of the Earth's space environment: an introduction*, Springer, Berlin.

Prölss, G. W., Brace, L. H., Mayr, H. G., Carignan, G. R., Killeen, T. L. and Klobuchar, J. A. (1991), 'Ionospheric storm effects at subauroral latitudes: a case study', *Journal of Geophysical Research* **96**(A2), 1275–1288.

Richmond, A. and Roble, R. (1979), 'Dynamic effects of aurora-generated gravity waves on the mid-latitude ionosphere', *Journal of Atmospheric and Terrestrial Physics* **41**(7–8), 841–852.

Rishbeth, H. (1989), F - region storms and thermospheric circulation, *in* P. Sandholt and A. Egeland, eds, 'Electromagnetic coupling in the polar clefts and caps', Kluwer Academic Publishers, pp. 393–406.

Rishbeth, H. and Garriott, O. K. (1969), *Introduction to ionospheric physics*, Academic Press, New York.

Rodger, A. S., Wrenn, G. L. and Rishbeth, H. (1989), 'Geomagnetic storms in the Antarctic F region II. Physical interpretation', *Journal of Atmospheric and Terrestrial Physics* **51**(11/12), 851–866.

Sahai, Y., Becker-Guedes, F., Fagundes, P. R., de Jesus, R., de Abreu, A. J., Paxton, L. J., Goncharenko, L. P., Brunini, C., Gende, M., Ferreira, A. S., Lima, N. S., Guarnieri, F. L., Pillat, V. G., Bittencourt, J. A. and Candido, C. M. N. (2009), 'Effects observed in the Latin American sector ionospheric F region during the intense geomagnetic disturbances in the early part of November 2004', *Journal of Geophysical Research* **114**(A3), A00A19.

Schunk, R. and Nagy, A. F. (2009), *Ionospheres: physics, plasma physics and chemistry*, 2nd edn, Cambridge University Press, Cambridge.

Seaton, M. (1956), 'A possible explanation of the drop in f-region critical densities accompanying major ionospheric storms', *Journal of Atmospheric and Terrestrial Physics* **8**(1–2), 122–124.

Seemala, G. K. and Valladares, C. E. (2011), 'Statistics of total electron content depletions observed over the South American continent for the year 2008', *Radio Science* **46**(5), RS5019.

South African Weather Service (2013), `www.weathersa.co.za/web/indexphp/corporate/education?id=216`. (Accessed 2013-10-28).

Ssessanga, N., Mckinnell, L. A. and Habarulema, J. B. (2014), 'Estimation of foF2 from GPS TEC over the South African region', *Journal of Atmospheric and Solar-Terrestrial Physics* **112**, 20–30.

Thomas, L. (1996), The coupling of the lower ionosphere with the mesosphere and lower thermosphere, *in* H. Kohl, R. Ruster and K. Schlegel, eds, '*Modern Ionospheric science*', European Geophysical Society, Katlenburg-Lindau, pp. 67–101.

Tsurutani, B. T., Gonzalez, W. D., Gonzalez, A. L. C., Guarnieri, F. L., Gopalswamy, N., Grande, M., Kamide, Y., Kasahara, Y., Lu, G., Mann, I., McPherron, R., Soraas, F. and Vasyliunas, V. (2006), 'Corotating solar wind streams and recurrent geomagnetic activity: A review', *Journal of Geophysical Research: Space Physics* **111**(A7), A07S01.

Tsurutani, B. T., Gonzalez, W. D., Gonzalez, A. L. C., Tang, F., Arballo, J. K. and Okada, M. (1995), 'Interplanetary origin of geomagnetic activity in the declining phase of the solar cycle', *Journal of Geophysical Research* **100**(A11), 21717–21733.

Uwamahoro, J. (2011), An analysis of sources and predictability of geomagnetic storms, PhD thesis, Rhodes university, Grahamstown.

Vijaya Lekshmi, D., Balan, N., Tulasi Ram, S. and Liu, J. Y. (2011), 'Statistics of geomagnetic storms and ionospheric storms at low and mid latitudes in two solar cycles', *Journal of Geophysical Research: Space Physics* **116**(A11), A11328.

Walker, A. (2005), *Magnetohydrodynamic waves in geospace: the theory of ULF waves and their interaction with energetic particles in the solar-terrestrial environment*, Institute of Physics Publishing, Bristol.

White, R. (1970), *Space Physics*, Gordon and Breach, New York.

Yao, Y. B., Chen, P., Zhang, S. and Chen, J. J. (2013), 'Temporal and spatial variations in ionospheric electron density profiles over South Africa during strong magnetic storms', *Natural Hazards and Earth System Science* **13**(2), 375–384.

Zhang, Y., Paxton, L. J., Morrison, D., Wolven, B., Kil, H., Meng, C.-I., Mende, S. B. and Immel, T. J. (2004), 'O/N2 changes during 1–4 October 2002 storms: IMAGE SI-13 and TIMED/GUVI observations', *Journal of Geophysical Research* **109**(A10), A10308.